Available online at www.sciencedirect.com
ScienceDirect
Deep-Sea Research I 54 (2007) 2036–2066
DEEP-SEA RESEARCH PART I
www.elsevier.com/locate/dsri

Deep western boundary current dynamics and associated sedimentation on the Eirik Drift, Southern Greenland Margin

Sally Hunter[a,*], David Wilkinson[a], Essyllt Louarn[b], I. Nick McCave[c], Eelco Rohling[a], Dorrik A.V. Stow[a], Sheldon Bacon[a]

[a]*National Oceanography Centre, Southampton, University of Southampton Waterfront Campus, European Way, Southampton SO14 3ZH, UK*
[b]*Laboratoire de Chimie Marine, UMR CNRS 7144 Roscoff and Institut Universitaire Europeén de la Mer/UBO, Place Nicolas Copernie, 29280 Plouzane, France*
[c]*Department of Earth Sciences, University of Cambridge, Downing Street, Cambridge CB2 3EQ, UK*

Received 29 March 2007; received in revised form 14 August 2007; accepted 11 September 2007
Available online 26 September 2007

Abstract

Growing interest in the dynamics and temporal variability of the deep western boundary current (DWBC) in the northern North Atlantic has led to numerous studies of the modern hydrography and palaeoceanography of this current system. The DWBC is fed by the two dense water-masses that spill over the Greenland–Iceland–Scotland Ridge; Denmark Strait Overflow Water (DSOW) and Iceland Scotland Overflow Water (ISOW). These overflows entrain ambient water masses, primarily Labrador Sea Water (LSW), as they cross the Iceland and Irminger Basins before merging in the vicinity of south-east Greenland. A number of studies have been performed around the Eirik Drift, located off the southern Greenland margin, downstream of this main merging point. However, the relationship between the DWBC and the associated sedimentation at this location has yet to be fully elucidated. New hydrographic data show that the current's main sediment load is carried by only one of its components, the DSOW. Seismic surveys and sediment cores confirm that Holocene sedimentation is limited to areas underlying the most offshore part of the current, where the hydrographic data show the highest concentration of DSOW. Active sedimentation through the Holocene therefore appears to have been controlled by proximity to the sediment-laden DSOW.

Our interpretation of new and historic geostrophic transport and tracer data from transects around the southern Greenland margin also suggests that the DWBC undergoes significant growth through entrainment as it flows around the Eirik Drift. We attribute this to multiple strands of ISOW following different depth-dependent pathways between exiting the Charlie Gibbs Fracture Zone and joining the DWBC. Comparison of our new data with other modern hydrographic datasets reveals significant temporal variability in the DWBC, associated with variations in the position, structure and age since ventilation of the current in the vicinity of Eirik Drift. The complexity of the current dynamics in this area has implications for the interpretation of hydrographic and palaeoceanographic data.

Keywords: Deep western boundary current; Eirik Drift; Hydrography; Sedimentation

*Corresponding author.
E-mail address: sallyh@noc.soton.ac.uk (S. Hunter).

0967-0637/$ - see front matter
doi:10.1016/j.dsr.2007.09.007

1. Introduction

The North Atlantic is separated from the Nordic Seas by the Greenland–Iceland–Scotland (GIS) ridge. The ridge plays a prominent role in shaping the ocean circulation of the region as it only allows waters down to intermediate depths to be exchanged between the two areas. The densest of these waters spilling south over the ridge are known as the overflow waters. Two key overflow waters, with distinctly different temperature and salinity characteristics cross the GIS Ridge to the west and east of Iceland; the Denmark Strait Overflow Water (DSOW) and Iceland Scotland Overflow Water (ISOW). Having crossed the GIS Ridge the overflow waters descend rapidly, following bathymetrically controlled pathways on route to their primary meeting point in the deep western boundary current (DWBC) off southeast Greenland, where this current is commonly referred to in the geological literature as the western boundary undercurrent (see Fig. 1).

During their journey through the Iceland and Irminger Basins the overflow waters entrain a combination of Labrador Sea Water (LSW) and modified Antarctic Bottom Water (known as Lower Deep Water—LDW). On reaching the Eirik Drift off the southern Greenland margin, the DWBC carries a combination of DSOW, ISOW, LSW and LDW that represents nearly mature (or proto) North Atlantic Deep Water (NADW). NADW is normally considered fully formed when the DWBC reaches the Grand Banks of Newfoundland after further additions of LSW, LDW and ISOW in the Labrador Basin. The DWBC off Cape Farewell, however, constitutes the major input to NADW. This input has been referred to as lower NADW (lNADW) in a growing number of modern physical oceanographic texts (e.g. Tanhua et al., 2005).

NADW spreads across the world's ocean floors forming one of the dominant constituents of the lower limb of the global thermohaline circulation (THC) system. The associated, density driven, component of the near-surface flow in the North Atlantic is responsible for significant poleward transport of heat, which helps to maintain the relatively moderate European climate (Ganachaud and Wunsch, 2000; Seager et al., 2002).

As research over the last few decades has increasingly focused on the role of the THC in shaping global climate (e.g. Broecker, 1991, 2000; Rahmstorf, 2000; Millwood et al., 2002), there has

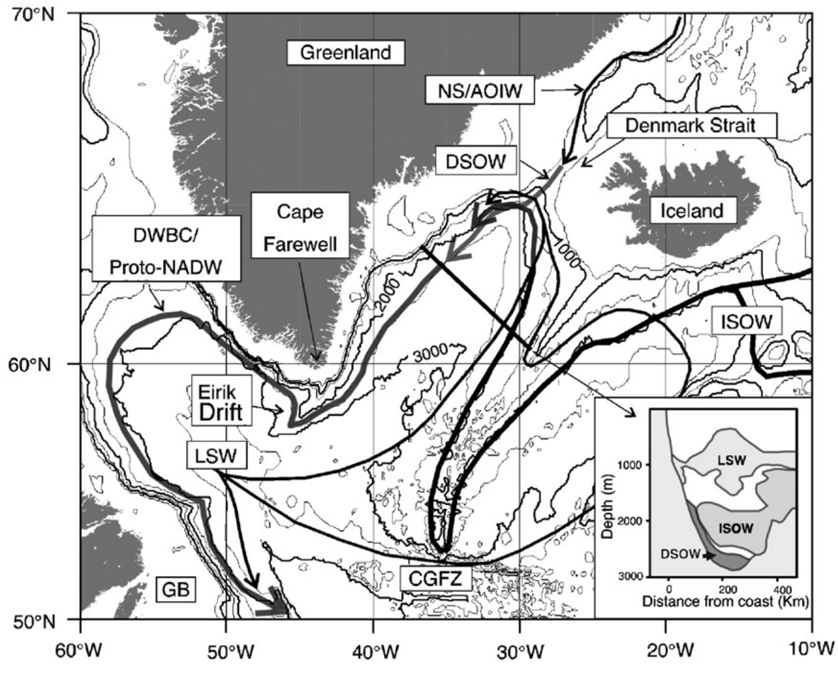

Fig. 1. Pathways of the main deep and intermediate water masses contributing to the DWBC. NS/AOIW, Norwegian Sea/Arctic Ocean Intermediate Water; DSOW, Denmark Strait Overflow Water; ISOW, Iceland Scotland Overflow Water; LDW, Labrador Sea Water. GB, Grand Banks; CGFZ, Charile Gibbs Fracture Zone. Inset from Dickson and Brown (1994).

been a growing interest in the mechanisms governing the rate of NADW formation and hence DWBC flux. The flux of the DWBC is known to have varied on time scales ranging from days (Clarke, 1984) to millennia (Bianchi and McCave, 1999), with the longer term variations thought to be intimately linked to climate-change events (e.g. Chamberlin, 1906; Broecker et al., 1985; Broecker, 2000; Rahmstorf, 2002).

The Eirik Ridge was first recognised as being constructed by deep currents, i.e. a sediment drift, by the group at Lamont Observatory in the late 1960s (Johnson and Schneider, 1969; Jones et al., 1970). The Eirik Drift contains an expanded sedimentary section, with sedimentation rates over 30 cm ka^{-1} in places (e.g. Hillaire-Marcel et al., 1994) making it suitable for high-resolution (decadal to millennial scale) studies of the current's variability. However, despite its importance as a record of DWBC variability, relatively little is known about the detailed relationship between current activity and sedimentation on the drift.

The aim of this investigation is to use a combination of geological and hydrographic techniques to determine the detailed water mass and velocity structure of the DWBC at the Eirik Drift and to determine the relationship between these features and the patterns of Holocene sedimentation. The results improve our understanding of DWBC activity at this important location, and so allow more informed interpretation of its sedimentary record.

2. Present day oceanographic setting

Clarke (1984) identified the DWBC in the Cape Farewell–Eirik Drift region as a bottom-intensified current that resides between the 1900 and 3000 m isobaths towards the foot of the continental slope. The DWBC transport is commonly accepted to be about 13–14 Sv (1 Sv = 1×10^6 m^3/s); for example, Dickson and Brown (1994) quote 13.3 Sv for the flow below the $\sigma_0 = 27.80\,\mathrm{kg\,m^{-3}}$ isopycnal. Although this figure is often cited, it is based largely on a single dataset collected in 1978 by the R.V. *Hudson* (Clarke, 1984). Bacon (1997) calculates a much lower value of 6 Sv from data collected in 1991 by the R.R.S. *Charles Darwin*, and Bacon (1998) argues that a comparison of data collected between 1958 and 1997 illustrates significant decadal variability of the DWBC due to changes in the output from the Nordic Seas.

Dickson et al. (1999) found that the relative warming of the subsurface waters of the West Spitsbergen Current during the winter of 1996–1997 resulted in a thinning and slowing of the DWBC in its lower reaches. They demonstrated that the extreme warmth of the overflow, causing it to run higher on the continental slope off east Greenland, could be reproduced in a numerical model that gave an upslope movement of the current core of between 15 and 20 km. Combining this result with the decadal variability inferred by Bacon (1998), it is clear that there is a high probability of significant inter-annual changes in the structure and position of the axis of maximum velocity of the DWBC.

2.1. Deep western boundary current water masses

Currently accepted values for DWBC water mass characteristics in the vicinity of southern Greenland are summarised in Table 1.

2.1.1. Denmark Strait Overflow Water

DSOW is composed of Nordic Sea intermediate waters that cross the Denmark Strait sill and then descend rapidly, entraining ambient waters, primarily LSW (Rudels et al., 2002). The resultant

Table 1
Typical water-mass characteristics for the components of the DWBC (Swift, 1984; McCartney, 1992; Dickson and Brown, 1994)

	Potential temperature	Salinity	Potential density[a]	Other
DSOW	<1.5	~34.9	>27. 88	High O_2
ISOW—Irminger Basin	1.8–3.5	~34.96–35.05	σ_2 36.95–37.05	Low O_2
ISOW—Near overflows	~−0.5	~34.92	~28.07	High O_2
LSW	~3–4	34.85	27.74–27.80	Low potential vorticity
AABW	~2		σ_4 46	Low O_2 High Si
NADW	2–3.5	34.88–34.98	>27.80	

[a]Referenced to surface (σ_0) unless otherwise stated. σ_2 = referenced to a depth of 2000 m and σ_4 = referenced to a depth of 4000 m.

modified DSOW is identifiable as the lower layer of the DWBC off Cape Farewell. The transport of DSOW across the sill and into the DWBC is estimated to be 2.9 Sv (Dickson and Brown, 1994), growing to around 10 Sv through entrainment along its route to Cape Farewell.

2.1.2. Iceland Scotland Overflow Water

ISOW is also composed of Nordic Sea intermediate waters, but with a significant component of Norwegian Sea Deep Water due to the deeper sills in the Iceland–Scotland Ridge to the east of Iceland. Dickson and Brown (1994) estimate the total overflow of ISOW to be about 2.7 Sv, of which 1.7 Sv flows through the Faeroe Bank Channel. The remainder of the overflow occurs via a series of five smaller channels between Iceland and the Faeroe Islands. The density of ISOW is reduced by entrainment of ambient waters as it travels around the Reykjanes Ridge and into the Irminger Sea via the Charlie Gibbs Fracture Zone (CGFZ), such that it forms the upper layer of the DWBC at a depth of around 2000 m. The contribution of this modified ISOW to the DWBC off Cape Farewell is estimated at between 2 and 3 Sv (Dickson and Brown, 1994; Schmitz, 1996).

2.1.3. Labrador Sea Water

LSW is formed by wintertime deep convection in the Labrador and Irminger Seas. As the name suggests, it was originally thought to be formed solely in the Labrador Sea, but more recent work has concluded that a second formation site exists in the Irminger Sea (Bacon et al., 2003; Pickart et al., 2003). LSW spreads across the North Atlantic and populates the low-velocity layer between about 700 and 1500 m off the east coast of Greenland. LSW contributes a significant proportion of the DWBC because of entrainment with the two types of overflow water. Dickson and Brown (1994) estimate the contribution of LSW to the DWBC at around 4 Sv off Cape Farewell, though inverse modeling has produced a figure as high as 8 Sv (Alvarez et al., 2004). This difference could be due to the high interannual variability in the production of LSW (Lazier et al., 2002), which model studies suggest may influence DWBC strength with a lag of 2–3 years (Eden and Willebrand, 2001).

2.1.4. Lower Deep Water/Antarctic Bottom Water (AABW)

Antarctic Bottom Water spreads north from its point of formation in the Antarctic and after modification joins the southward flowing DWBC at various points in the North Atlantic. In its modified North Atlantic form, it is nowadays properly referred to as LDW (McCartney, 1992). It is estimated that 1–2 Sv of LDW joins the DWBC off Greenland (Schmitz and McCartney, 1993; Schmitz, 1996), with a further 2 Sv thought to be entrained along the path of the DWBC around Newfoundland and Florida.

3. Geological setting and drift morphology

Significant drift building began off the southern Greenland Margin in the Early Pliocene (~4.5 Ma) linked to intensification in the flow of northern sourced bottom waters, which had begun overflowing from the Denmark Strait in the Late Miocene (Arthur et al., 1989). Active drift construction during the Pliocene was followed by more aggradational sedimentation in the Pleistocene as bottom currents weakened (Arthur et al., 1989). The drift is now generally considered to largely be a relict feature (Hiscott et al., 1989), but thick Holocene sediments do occur at the drift toe (Hillaire-Marcel et al., 1994).

The morphology of the drift is strongly influenced by basement structure (Hillaire-Marcel et al., 1994; Hunter et al., 2007). The drift extends obliquely from the Greenland margin with the crest deepening from 1500 m in the north, adjacent to the margin, to around 3400 m at the drift toe, some 360 km to the southwest (Fig. 2a). The southern flank of the drift lies below the southwest-flowing limb of the DWBC in the Irminger Sea and is characterised by a relatively steep and regular slope of around 1.3° that follows basement topography. The northern drift flank and drift crest display marked changes in slope, with variations between 0.3° and 1.5° defining three secondary ridges (Figs. 2a and b), which extend to the northwest from the main drift crest and underlie the DWBC as it flows northwest into the Labrador Sea. These secondary ridges approximately overlie basement highs, which are postulated to have controlled their original development (Hunter et al., 2007).

The deepwater drift toe between around 3000 and 3500 m displays a marked decrease in the angle of slope from the southern to northern drift flank (shown by the increase in bathymetric contour spacing from south to north in Fig. 2a). A number of local topographic variations occur within this area including two newly discovered seamounts

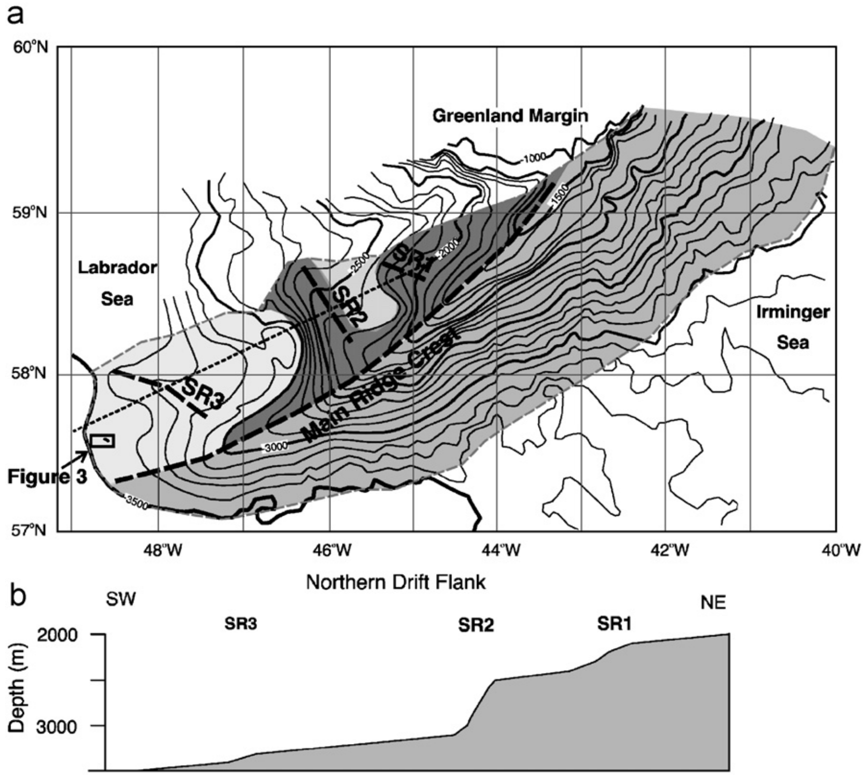

Fig. 2. (a) Bathymetric map of the Eirik Drift with the main ridge crest and secondary ridge crests (numbered SR1–3) indicated (Modified from Hunter et al., 2007). For the northern drift flank, darker shading indicates areas of steeper slope and (b) schematic cross-section of the northern drift flank (section line indicated on 2a) showing the relative magnitudes of the secondary ridges.

(located at 57°34.5′N 48°38′W and 58°31.5′N 48°27′W). Swath bathymetry shows the southern seamount to be an elongate feature trending NW–SE with steep sides and a maximum elevation of around 140 m above the surrounding sea floor (Fig. 3). The seamounts are associated with shallow moats, presumably related to local current intensification, and are assumed to represent basement highs similar to those seen in regional seismic sections (e.g. Srivastava et al., 1989).

4. Hydrography of the Cape Farewell–Eirik Drift Region

4.1. Hydrographic data

Our interpretation of the present-day physical oceanography of the Cape Farewell region is based upon two hydrographic datasets. The primary dataset is a series of new data collected between the 1st and 17th of September 2005 by R.R.S. *Discovery* cruise D298 (Bacon, 2006). The D298 data provide five hydrographic sections around and over the Eirik Drift (Fig. 4a). These sections (referred to as D1–D5 throughout this text) provide high-resolution temperature and salinity data, allowing the construction of detailed geostrophic current cross-sections. In combination with oxygen concentration (to give an indication of age since ventilation), light transmittance (providing an estimate of fine-grained sediment load) and silicate concentration (to track the pathways and admixtures of LDW), the geostrophic velocity cross-sections offer a deeper understanding of the current dynamics in the region.

The second dataset consists of historical data from the World Ocean Database (WOD) (Conkright et al., 2002). Thirteen sections (referred to as H1–H13 throughout this text) were selected from the WOD that could provide high-resolution temperature and salinity sections in the vicinity of Cape Farwell. Some of these sections also provided oxygen concentration data, but unfortunately there are no transmittance data and only limited silicate concentration data on the WOD. The cruises that provided the historical data are listed

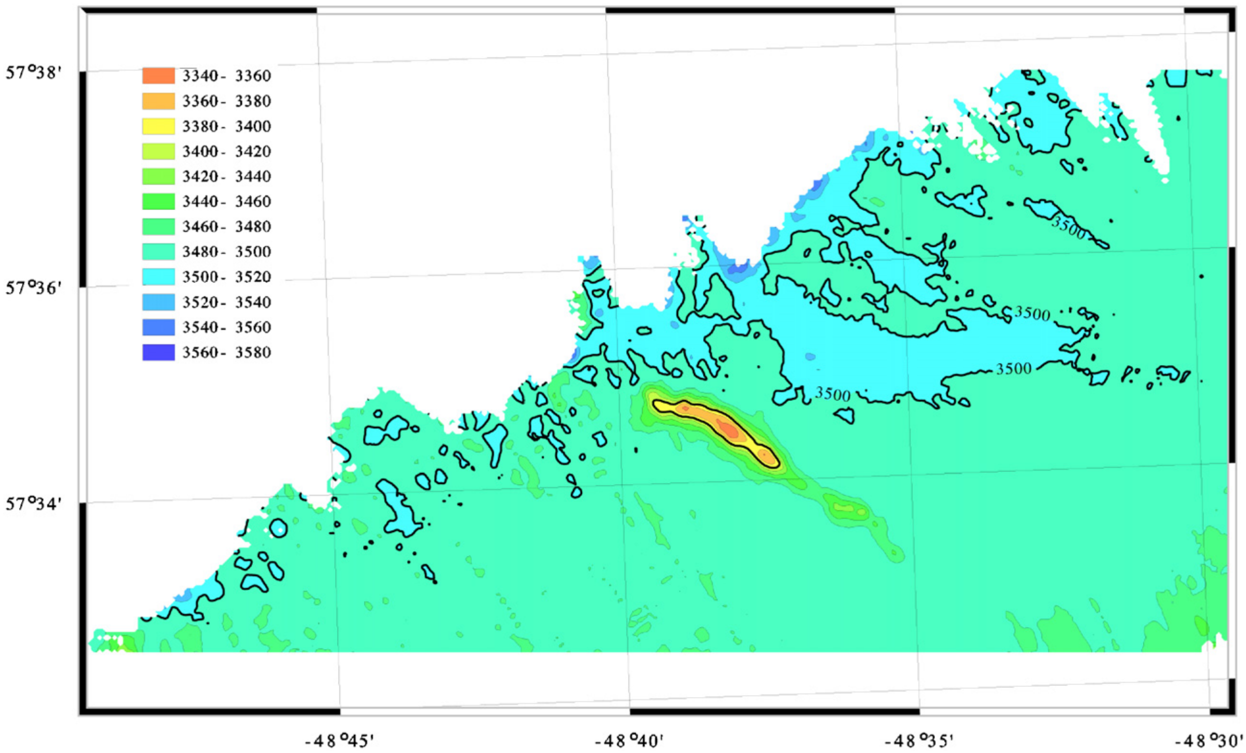

Fig. 3. Swath bathymetric map of the southern of the two newly discovered seamounts. Location shown in Fig. 2.

in Table 2, and the locations of the transects are shown on Fig. 4a.

4.2. Hydrographic methods

To understand the relationship between the DWBC and sedimentation patterns requires a detailed understanding of the current's velocity structure both in cross-section and as it travels around the Eirik Drift. However, the use of CTD data to calculate geostrophic velocities in the DWBC presents a number of challenges. Firstly, there are the standard problems of determining a reference velocity and the absence of information on the component of the current parallel to the section. The fact that the DWBC is a bottom-following current of around 500 m in thickness (Clarke, 1984) lying above a sloping sea floor creates additional problems. The standard geostrophic calculation produces an inter-station average along a level surface and the typical station separation (~10 km) will result in this averaging effect covering sections of the water column that are both inside and outside the main current (Fig. 5).

Despite the above drawbacks, the calculation of geostrophic velocity shears still provides the best method for determining the structure of the DWBC from the available data in this region. The geostrophic approach also has the advantage over direct current measurement that there is an inherent degree of spatial and temporal averaging.

Within the area of the DWBC, water temperature, salinity and velocity typically vary as a function of distance above the bottom rather than depth. Clarke (1984) used this feature to calculate velocities and transports in the bottom triangle between two stations created by the sloping bottom. We have employed the same technique to calculate bottom triangle velocities and to improve the horizontal interpolation of the data. All water-mass tracers were linearly interpolated onto a 2 km grid along lines of equal height above the seabed for the lower 600 m of the water column. This seafloor following grid was then spliced to a standard horizontally interpolated grid for the upper section of the water column. This simulates high-resolution data to create more realistic contour plots as well as temperature and salinity grids for the calculation of geostrophic velocities.

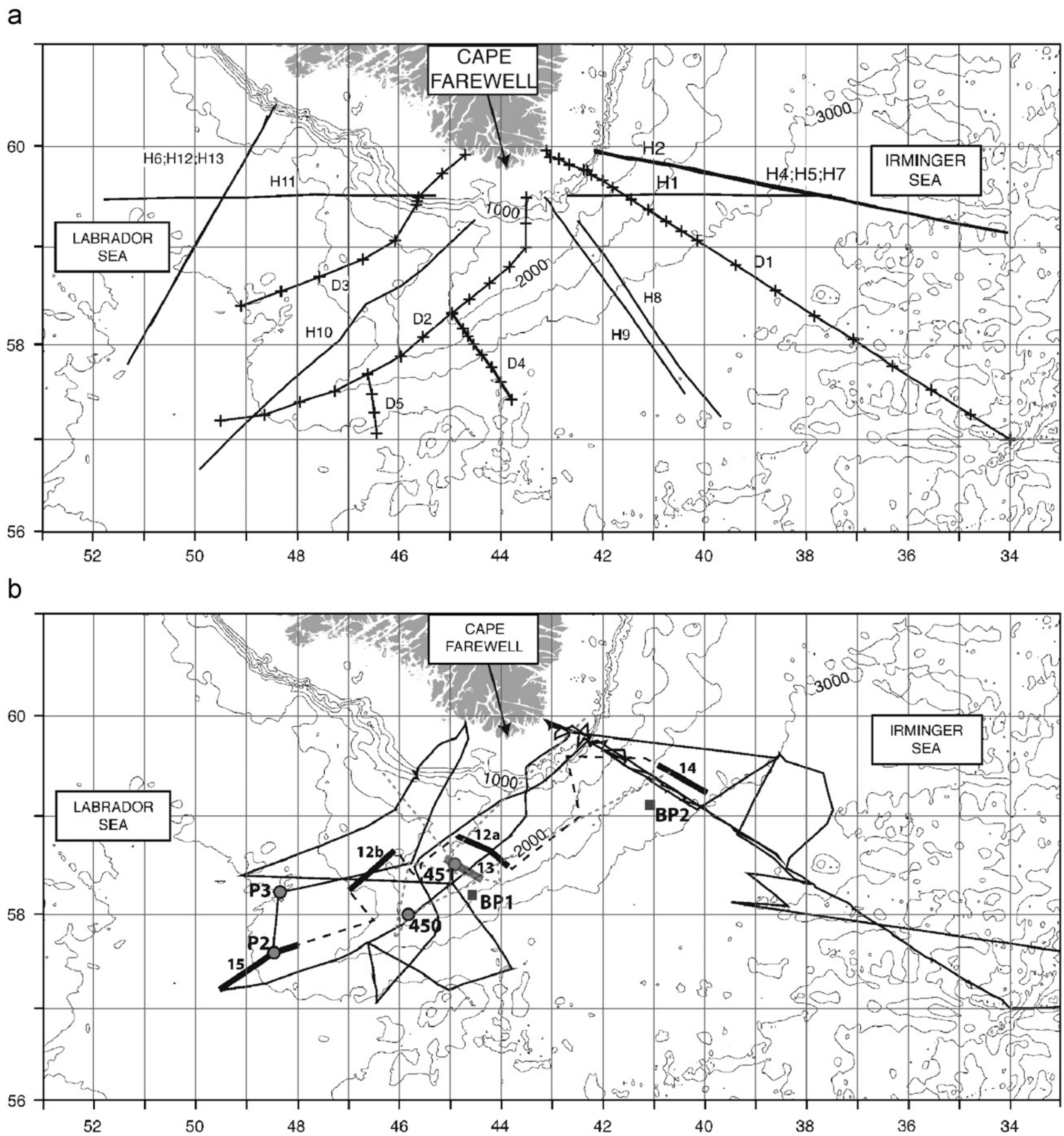

Fig. 4. (a) Location of hydrographic data. The D298 and WOD hydrographic sections are numbered as outlined in the text. For the D298 sections, the crosses indicate the positions of the CTD stations and (b) location of geological and geophysical data. Profiler lines from cruise D298 are shown by the solid black lines, from CD159 by the dashed black lines and from TTR-13 by the dashed grey lines. The position of sidescan sonar line makat-86 (Fig. 13) is indicated by the solid grey line. Cores TTR13-450 and TTR13-451, D298-P2 and D298-P3 are labelled 450, 451, P2 and P3, respectively. The locations of Figs. 12, 14 and 15 are indicated in black along with the positions of the bottom photographs (BP1 and BP2) shown in these figures (from Rabinowitz and Eittreim, 1974).

The method chosen to extrapolate data into the bottom triangles has been shown to be of significance when calculating transports for bottom intensified currents flowing across a sloping bottom (e.g. Fiadeiro and Veronis, 1983). In the case of the D298 sections, the bottom triangles contribute

Table 2
Source of World Ocean Database historic sections

Reference	Date	Country	Ship	WOD Cruise ID
H1	March/April 1962	USA	*Erika Dan*	WOD01_31000170
H2	November 1994	UK	*Charles Darwin*	WOD01_74009777
H3	September 1991	Germany	*Meteor*	WOD01_06009866
H4	September 1992	Germany	*Valdivia*	WOD01_06009201
H5	November 1994	Germany	*Meteor*	WOD01_06009630
H6	June 1995	Germany	*Valdivia*	WOD01_06009881
H7	August 1996	Germany	*Valdivia*	WOD01_06009883
H8	November 1994	UK	*Charles Darwin*	WOD01_74009777
H9	November 1996	USA	*Knorr*	WOD01_31014521
H10	February 1962	USA	*Erika Dan*	WOD01_31000170
H11	March 1962	USA	*Erika Dan*	WOD01_31000170
H12	May 1994	Canada	*Hudson*	WOD01_18012901
H13	May 1997	Canada	*Hudson*	WOD01_18012902

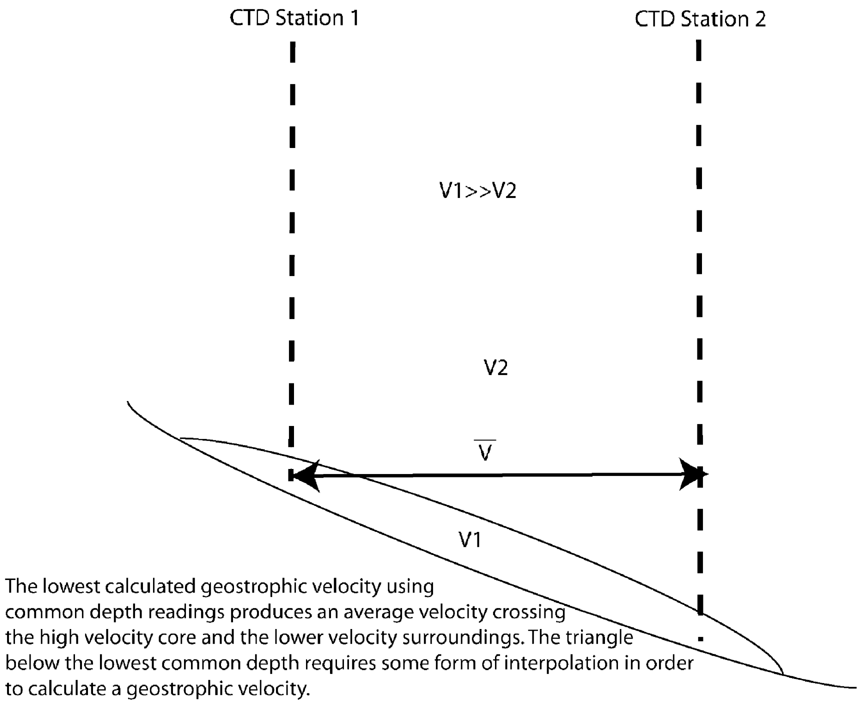

Fig. 5. Schematic demonstration of the problems associated with the calculation of geostrophic current velocities for a bottom-intensified current on a sloping bottom.

between 25% and 30% of the total cross-section transport. Our methodology produces values that are intermediate to those produced by taking a constant velocity and a constant vertical shear from the lowest common depth between station pairs. In line with the observations of Fiadeiro and Veronis (1983) our values lie much closer to those using a constant velocity, being 0.2–0.5 Sv higher. For the purposes of this paper we are primarily interested in spatial transport patterns employing a consistent and reasonable approach to the transport calculation. We therefore believe that, in this case, the uncertainties due to the extrapolation methodology are immaterial.

In order to calculate DWBC transports it is first necessary to select a reference velocity. In the absence of any direct current measurement data it is usual to set a level of no motion somewhere between 1000 m (e.g. Bacon, 1998) and 1500 m (e.g. Clarke, 1984). Although historical current metre data from the region suggest that the mid-depth velocity minimum is not zero (Clarke, 1984), the accepted range of values for the DWBC transport constrains the velocity to be no more than a few $cm\,s^{-1}$. The maximum potential reference level offset is small in comparison with the near bottom velocities, of around $20\,cm\,s^{-1}$, obtained by depth integration of the baroroclinic shears. Therefore the uncertainty in the reference level does not significantly impact on our use of this method to determine the location and structure of the current. In the absence of direct current measurement data we have selected 1500 m as a level of no motion based upon the shear structure seen in the data.

The second decision required in the calculation of DWBC transports concerns the proportion of the water column we attribute to the DWBC. Other authors have typically taken the transport below a particular potential density surface (e.g. $\sigma_0 = 27.8\,kg\,m^{-3}$—Bacon, 1998). The work by Dickson et al. (1999), which demonstrates the inter-annual variability in the temperature and density of the current, raises questions over this approach when results from different years are compared. We have therefore chosen the simpler approach of attributing all transport below the level of no motion to the DWBC. Again the inferences we make are not particularly sensitive to this decision, and our aim is to combine reasonable transport estimates with tracer and sedimentation data in order to develop a coherent picture of current and sedimentation dynamics in the region.

Light transmittance data acquired during R.R.S. *Discovery* cruise D298 have been used to identify variations in turbidity within the water column in order to assess the distribution of sediment load. The principles behind the formation and identification of turbid bottom nepheloid layers are not discussed in detail here, but see McCave (2003) for a review.

The transmittance (T) data were converted to beam attenuation coefficient (c) using the equation:

$$c = (\ln(1/T))/l$$

with path length $(l) = 0.25\,m$.

Drift in the transmissometer calibration between stations has been corrected by setting the minimum recorded beam attenuation to 0.37 for each station profile. This approach is reasonable for identifying the signals seen in the DWBC as the magnitude of the variation seen across the current far outweighs the spatial variation that can be expected in the clear water minimum over the area of the survey. The beam attenuation data are not interpreted as a quantitative proxy for suspended particulate matter (SPM) concentrations because of a lack of actual SPM measurements for calibration and the necessity to prescribe the minimum beam attenuation value of 0.37 at each station. The transmittance data do, however, provide an adequate basis for the assessment of the location and structure of nepheloid layers, and for process-based interpretations of their development (Spinrad and Zaneveld, 1982; McCave, 1983, 2001; Gardner et al., 1985).

Oxygen concentrations measured on cruise D298 and obtained from the WOD were converted to saturations with reference to solubilities calculated according to the temperature and salinity relationships of Weiss (1970).

Samples for silicate analysis were taken at each of the D298 CTD stations at a sub-set of depths chosen to characterize the different water masses. The samples were frozen for the transfer to the Laboratoire de Chimie Marine (Roscoff), where they were analysed on a Bran and Luebbe AutoAnalyzer II.

4.3. Interpretation of D298 water-mass tracers and current profiles

The DWBC is marked in all five D298 sections by a near-bottom reduction in temperature and salinity. The relatively young DSOW is further differentiated by an increase in oxygen saturation in comparison with the ISOW and LSW above. The current extends out slightly beyond the centre of the Irminger Basin in section D1 (ca. 270 km along the section) and then deepens with the bathymetry as it passes around the Eirik Drift. The current was seen to reach further into the basin than expected on sections D2–D5, extending beyond the most offshore station in each case. Closer inspection reveals a number of more detailed features.

The velocity plots (Fig. 6a) show the core of the current to be situated towards the bottom of the slope with a lower velocity tail extending out into the abyssal plains. Sections D1 and D2 show the possible presence of a separate current strand at a bottom depth of around 2000 m. This is a feature that is more prevalent in the historic sections and could be indicative of a separate ISOW pathway. This is discussed further in Section 5.2.

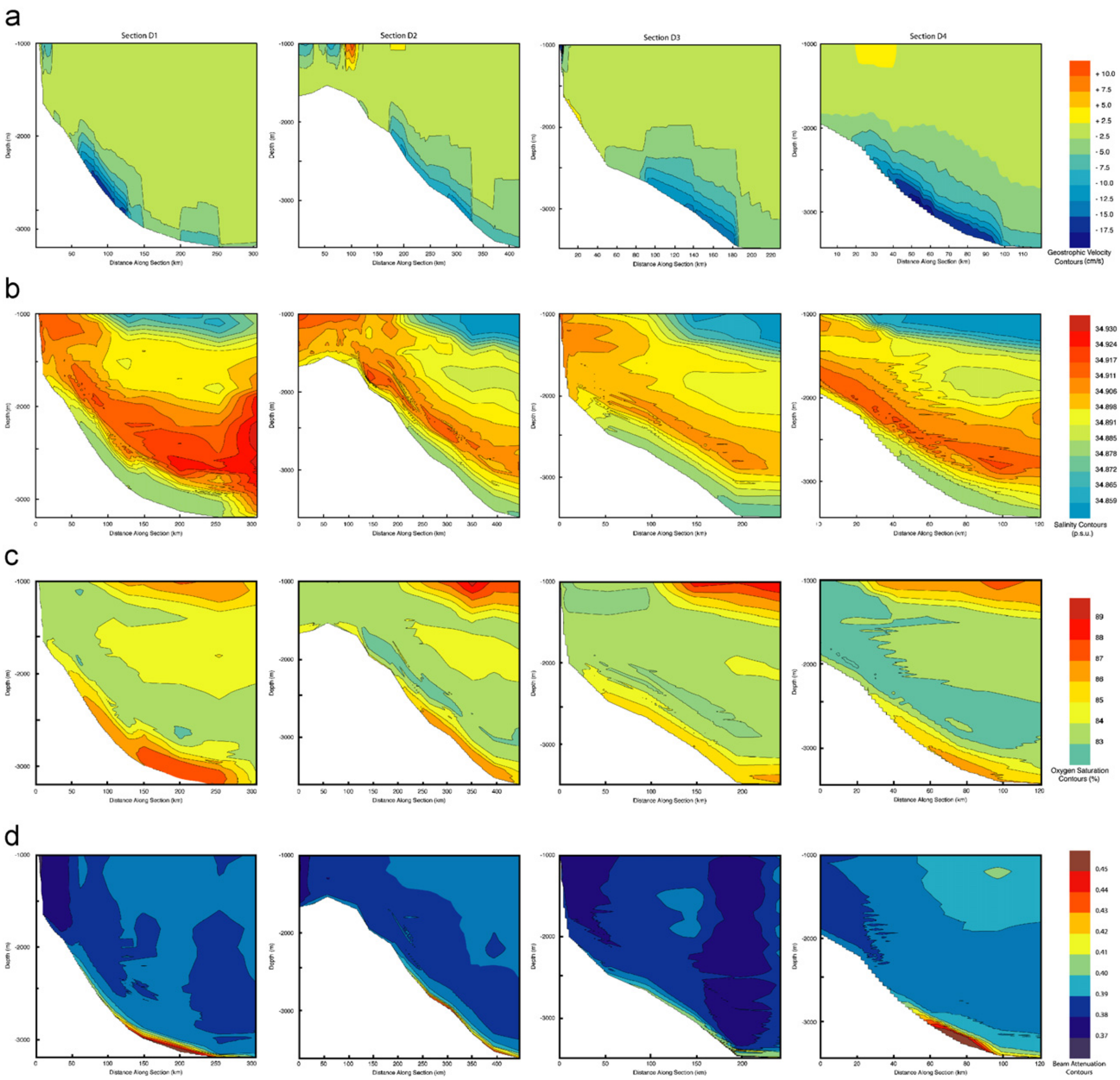

Fig. 6. Geostrophic velocity and water property contour plots for the D298 sections: (a) geostrophic velocity contour plots with contour spacing of $2.5\,\mathrm{cm\,s^{-1}}$ (excluding zero). Negative velocities represent clockwise flow around Cape Farewell; (b) salinity contour plots with contour spacing of 0.065; (c) percentage oxygen saturation contour plots with contour spacing of 1% and (d) beam attenuation contour plots with contour spacing of $0.01\,\mathrm{m^{-1}}$.

The quantitative interpretation of the calculated geostrophic velocities and transports (Table 3) requires some care, as they do not represent total transports or actual maximum velocities. Subject to the normal caveats on geostrophic equilibrium and reference level, the transports represent the total baroclinic flow provided that the sections cross the entire width of the current. The calculated maximum current speed, however, is affected by the angle at which the section crosses the current and will be underestimated by a factor of the sine of this angle. This in particular affects the maximum velocity seen in section D2 ($12\,\mathrm{cm\,s^{-1}}$). Maximum current velocities in the perpendicular sections D4 and D5 (23 and $22\,\mathrm{cm\,s^{-1}}$, respectively) are greater than those in D2 by a factor of at least 2. This suggests that section D2 is at a low angle to the current relative to sections D4 and D5.

Table 3
Summary results from D298 geostrophic velocity calculations

Section	Baroclinic transport below 1500 m (Sv)	Maximum velocity below 1500 m (cm/s)	Maximum station depth (m)
D1	5.7	17	3202
D2	10.0	12	3614
D3	8.3	14	3498
D4	6.8[a]	23	3435
D5	9.0[a]	22	3563

[a]These transports combine the transports calculated from the short sections D4 & 5 with the appropriate portion of section D2 to extend them to the inshore side of the DWBC.

The D298 data, collected over a period of less than 3 weeks, show significant variability in the transport. This variability could be due to short-term temporal variability in the actual DWBC transport, geographic or temporal variability in the reference level current (resulting in a baroclinic variability that is higher than the variability in the true transport) or flow into or out of the current zone between sections. It is likely that all three mechanisms play some role. It is also worth noting that the variation in transports seen between the sections varies in line with the maximum depth to which each section extends. In some cases this is a function of bathymetry (i.e. D1 extends to the maximum depth of the Irminger Basin at this latitude), but in others (D4 and D5) it is in part due to the length of the section being a little short. The latter could explain the relatively low transport calculated for D4 (i.e. the transport is actually higher, but the section was not long enough to capture it all).

The limited direct current measurement data that are available do show high short-term temporal variability at a single location. For example, mooring data for the DWBC off Cape Farewell collected in early 1978 (Clarke, 1984) show 100% variability in mean current speeds for consecutive 7-day periods. It is therefore possible that the variability we have observed in baroclinic transport (Table 3) is due entirely to temporal variations in the actual DWBC transport. We should also consider that the very location-specific nature of current meters could produce temporal variability in their records that is removed by the spatial averaging effect of the geostrophic calculation. The interannual movements in the current position observed by Dickson et al. (1999), if repeated over much shorter time periods, could produce much greater variability in current-metre records than is actually present in the DWBC transport. This type of variability may be a common feature of the DWBC as it was demonstrated farther downstream in HEBBLE by Hollister and McCave (1984) and Gross and Williams (1991).

Alternatively, small variations in the reference level velocity could offset the observed baroclinic transport variability. The low baroclinic transport calculated for section D1 (Table 3) could suggest a higher reference velocity at 1500 m on the entry to the drift, whereas the 10 Sv calculated for section D2 may suggest little or no barotropic component. The Dickson and Brown (1994) DWBC transport of 13.3 Sv is relatively high in comparison to the baroclinic transports we have calculated and those of Bacon (1998); however, to bring the transport in section D1 to a similar level only requires a reference level velocity of 3.8 cm s^{-1} (assuming the DWBC is 200 km wide and on average 1000 m in vertical extent).

More interestingly water-mass tracer data suggest that at least part of the observed geographic variation in baroclinic transport results from the entrainment of additional water masses on the entry to the Eirik Drift (between sections D1 and D2/D4/D5). This is discussed in more detail in the following paragraphs.

The water-property contour plots show a clear relationship between high oxygen saturation, low salinity and high beam attenuation within the core of the DWBC in all five D298 sections (Figs. 6b–d). The beam attenuation data define a distinct bottom nepheloid layer that is around 300 m thick and most strongly developed where the sea floor drops below 2800 m (Fig. 6d). Cross-plotting the salinity and oxygen saturation data for the interval of the DWBC with the beam attenuation shown by colour (Fig. 7a) confirms this relationship without any influence from the interpolation and contouring routines employed in creating Fig. 6. The oxygen saturation high within the DWBC, seen near the base of the continental slope in each section, can be interpreted as the zone of purest or youngest DSOW, as this has a shorter travel time from the point of surface contact than ISOW (e.g. Smith et al., 2005). This is supported by the lower salinity, consistent with DSOW. The higher beam attenuation values in waters of high oxygen saturation and low salinity imply that DSOW is carrying a higher load of the fine sediment (to which the

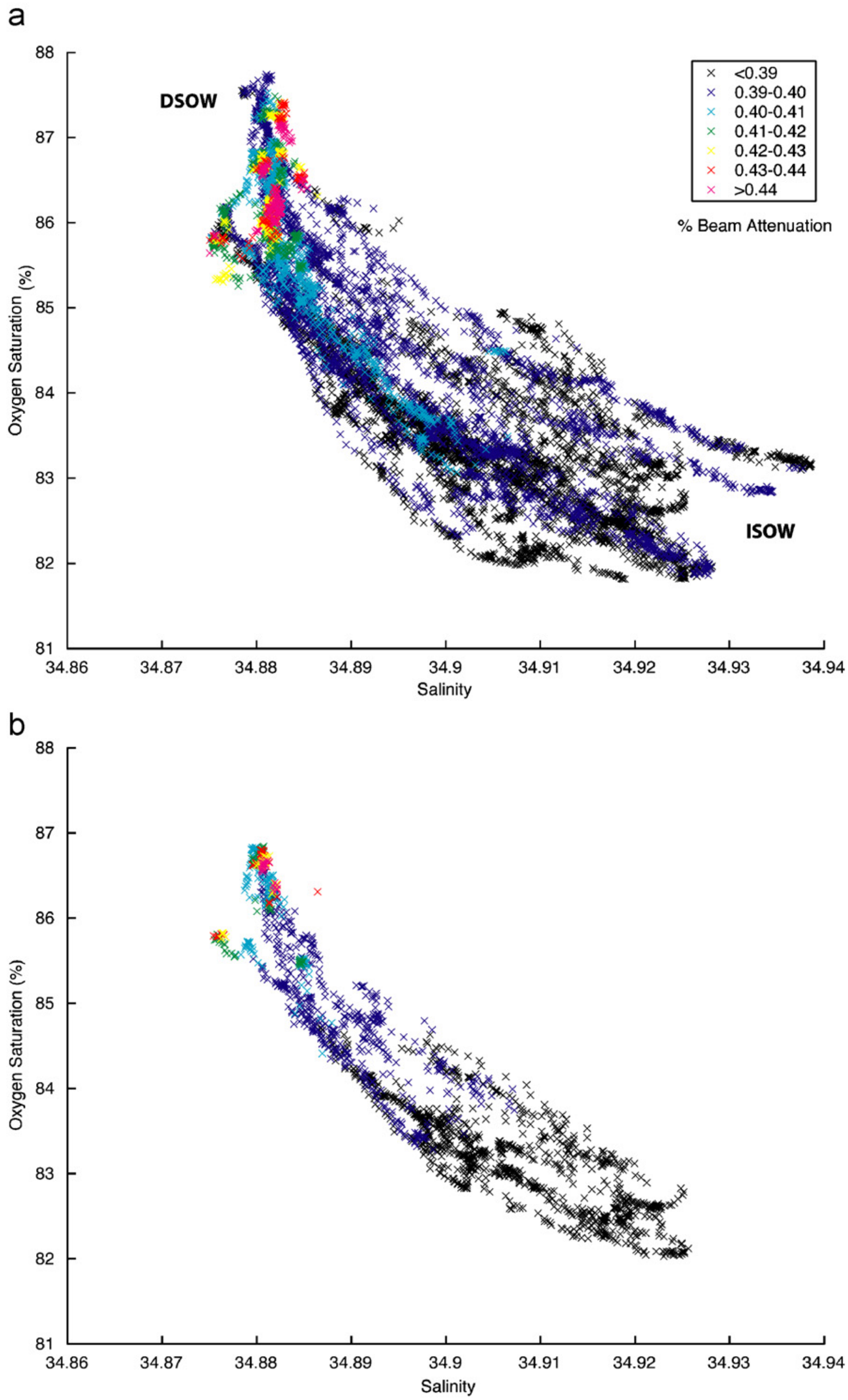

Fig. 7. Cross-plots of salinity versus oxygen saturation for: (a) all D298 sections and (b) section D2.

transmissometer is sensitive) than the other water masses within the DWBC. Comparing beam attenuation and velocity sections (Figs. 6a and d) it appears that the area of highest sediment load does not coincide with the area of highest current speeds. This would agree with the earlier observation that sediments along the deep-water eastern margin of Greenland can be traced to sources in east

Greenland and are therefore linked to transport by the DSOW (Innocent et al., 1997).

Our comparison of sections D1 and D2 suggests the addition of new components to the DWBC between these sections. The offshore extent of the DWBC in section D1 is marked by a decrease in oxygen saturation combined with an increase in salinity (Figs. 6b and c), which is consistent with the transition from majority DSOW to a higher percentage of older, high-salinity ISOW. Conversely, the offshore end of the DWBC in section D2 shows a decrease in oxygen saturation combined with a decrease in salinity (Figs. 6b, c and 7b). Although short-term variability in the salinity of the current cannot be excluded, the appearance, in section D2, of salinities lower than those seen anywhere in section D1 does strongly suggest the addition of a new component.

Two "candidate" water masses of low salinity and reduced oxygen saturation have been previously identified in this area. Smith et al. (2005) suggest that there is a component of re-circulating DSOW in the Irminger Basin. This could add a different vintage of DSOW with reduced oxygen saturation and a slightly different salinity to the DWBC in the vicinity of section D2. A re-circulating stream of DSOW lying to the south of section D1, but crossing D2, could also enhance the transport seen at section D2 if the outer arm of the recirculation was in the middle of the Labrador Basin beyond the offshore end of section D2. The second potential low salinity and oxygen saturation source is LDW, which has a substantial AABW component (McCartney, 1992; Dickson et al., 2002; Smith et al., 2005). The addition of LDW to the DWBC between sections D1 and D2 could result from the entrainment of LDW that has travelled directly up the western basin of the Atlantic or from a deeper component of ISOW, below about 3200 m, that has taken a more direct route across the Irminger Basin, omitting section D1 from its path. McCartney (1992) has shown that the proportion of LDW in ISOW increases with depth as shown by increasing silicate concentration in data collected from either side of the Reykjanes Ridge. The elevated silicate concentration signature in LDW, due to its AABW component, provides a good way of tracking its flow.

A cross plot of silicate concentration versus salinity (Fig. 8), combined with silicate concentration depth profiles (Fig. 9), for the D298 data provides some interesting insights into the movement of AABW in the region. The pattern of data seen in Fig. 8 is consistent with mixing between 3 end members: DSOW with low salinity and low silicate (ca. 33.88 and 8 μmol/l), ISOW with high salinity and low silicate concentration (>34.95 and ca. 10 μmol/l) and LDW with an intermediate level of salinity but high silicate concentration (ca. 34.92 and 17 μmol/l). The lines M1, M2 and M3 are suggested mixing results for combinations of ISOW and DSOW, DSOW and LDW, and ISOW and LDW, respectively.

In the eastern Irminger Basin (stations 3–5) silicate rich ISOW flows northwards with its proportion of LDW increasing with depth as indicated by the downward increase in silicate concentration and fall in salinity (Figs. 8 and 9). The data from these stations define mixing line M3. In the western Irminger Basin, the silicate maximum is displaced upwards by the southward flowing DSOW (stations 6–17 along section D1), and in the region of the main current it is typically 500–600 m above the bottom near the upper surface of the main DWBC. Data from stations 6–17 lie broadly along mixing line M1 and would therefore suggest mixing between DSOW and the deeper elements of the Irminger current flowing around the Reykjanes Ridge.

Following the path of the DWBC around Cape Farewell, the majority of data from sections D2–D5 appear above mixing line M1, which would support the addition of silicate rich water that was not present anywhere along section D1. Silicate concentrations towards the offshore end of the DWBC in sections D2 and D4 are slightly elevated in comparison with the same part of the current in section D1, whereas a reduction ought to have been expected if there were no additions and continued mixing. Instead, the highest silicate concentrations in the dataset are found in section D4 at the upper edge of the current in water depths of between 2000 and 2500 m. This high silicate concentration zone is seen to continue around Cape Farewell with a slight reduction in values from section D1 to sections D2 and D3.

The silicate data therefore support the concept of entrainment of new water masses between sections D1 and D2 in two areas along the upper surface of the current; one at the foot of the DWBC in water depths of between 3000 and 3500 m, and the other near the upslope end of the current in water depths between 2000 and 2500 m. The first addition would be consistent with the flow of the deepest, most

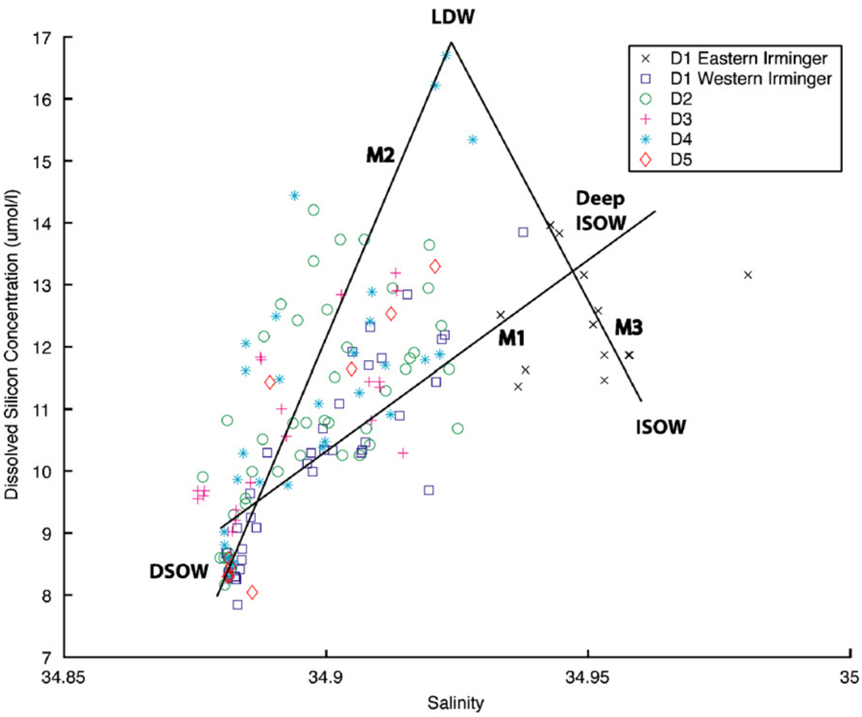

Fig. 8. Plots of salinity versus silicate concentration for all D298 samples taken within 600 m of the bottom and in water depths of over 1500 m. M1 and M2 represent suggested mixing lines between DSOW and ISOW and between DSOW and Western Basin LDW. M3 represents mixing between ISOW and LDW in the eastern basin of the North Atlantic.

silicate rich component of the ISOW through the CGFZ and across the Irminger Basin at depths greater than 3200 m (McCartney, 1992). However, the intersection of lines M2 and M3 in Fig. 8 suggest that, while this may explain the increase in silicate concentration it cannot alone explain the observed reduction in salinity. The second addition, where the highest silicate concentrations were observed, is too high in the water column to be consistent with ISOW exiting the Gibbs Fracture Zone. This agrees with the observations of McCartney (1992), who shows that silicate concentrations of greater than 16 μmol/l carried by ISOW fail to penetrate northwestward through the Irminger Basin. We therefore infer that the second, shallower, region of silicate addition observed in section D2 results from mid-depth spreading in the western basin of an intermediate water mass with a component of Antarctic origin.

4.4. Comparison with historic sections from the World Ocean Database

Although the 13 historical sections extracted from the WOD are too few to comment with authority on inter-annual variability in the transport of the DWBC, some interesting comparisons can be made with the calculated D298 transports. Sections H1, H10 and H11 (1962 bottle data) lie in a similar geographic configuration to sections D1–D3 (Fig. 4a) and were collected over a similarly short period of time. The 1962 results repeat the D298 pattern of low transport at section D1 in the Irminger Basin, with increased transport in the Labrador Basin, and with highest transport over the Eirik Drift (Tables 3 and 4).

Although the similarity between these two regional surveys is insufficient to conclusively characterise the spatial and temporal variability, the repeat of the spatial pattern between 1962 and 2005 does hint that temporal variability may not fully explain the increase in transport between the Irminger Basin and the Eirik Drift. It could also lend credence to the suggestion that some of the variability seen in current-metre-based data results from short-term movements in the position of the current. To resolve this issue ideally requires detailed analysis of synchronous, high-resolution mooring, bottom mounted ADCP and CTD data. However, we shall consider the hypothesis that the observed pattern is, to some extent, a regular feature. This would leave

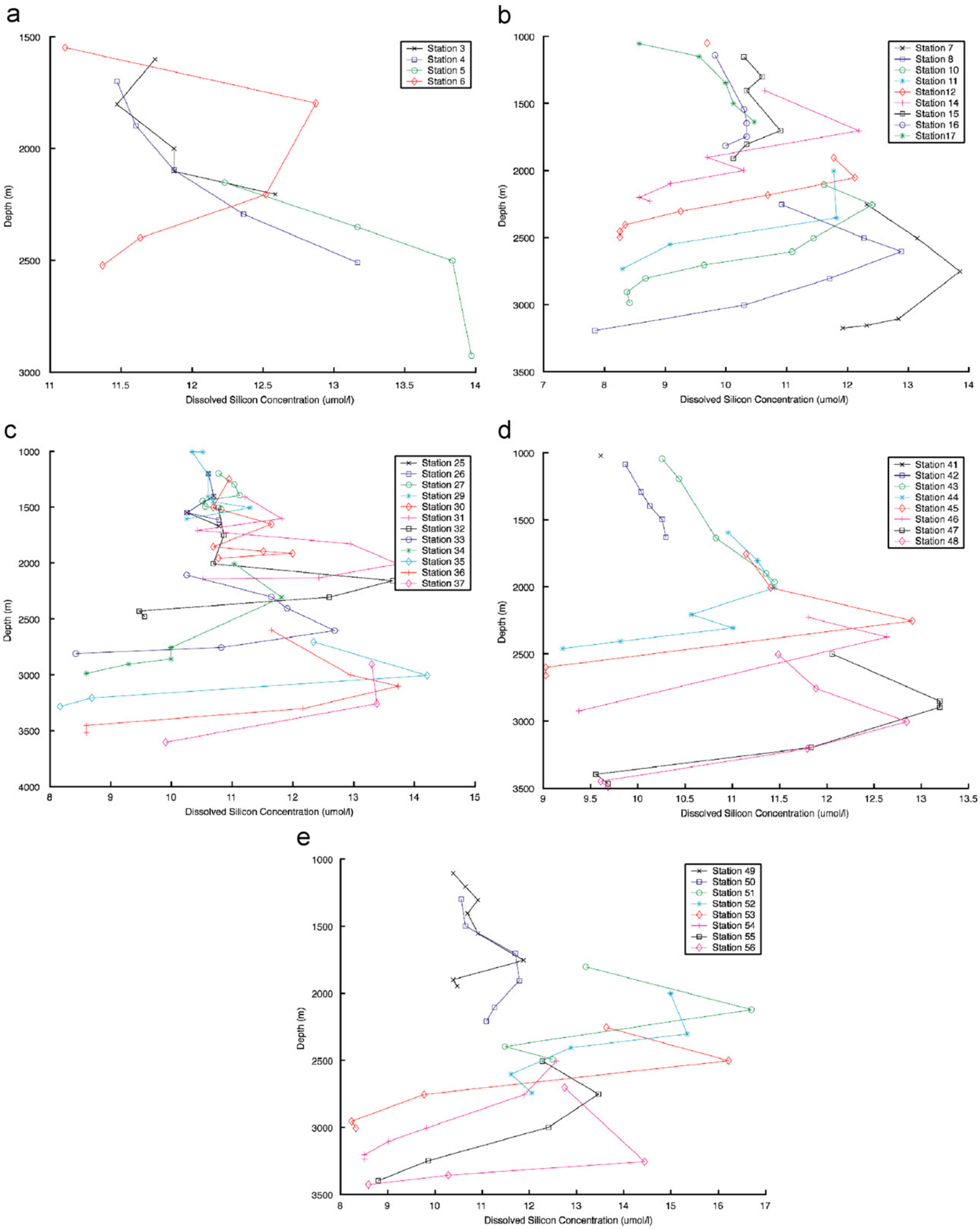

Fig. 9. Depth profiles of silicate concentration for D298 sections D1–D4 with section D1 split approximately in the centre of the Irminger Basin. Data are plotted for samples taken within 1000 m of the bottom in depths of over 1000 m.

Table 4
Summary of transport and DWBC water characteristics for the historic sections in comparison with D1

Section	Baroclinic transport (Sv)	DWBC salinity minimum	Bottom depth at DWBC salinity minimum (m)	DWBC salinity maximum	Bottom depth at DWBC salinity maximum (m)
D1	5.7	34.879	3202	34.939	3190
H1	5.1	34.881	2897	34.954	3106
H2	5.1	34.876	2715	34.939	3185
H3	4.8	34.880	3129	34.945	2861
H4	5.5	34.873	2606	34.943	3114
H5	4.6	34.859	2955	34.936	3130
H6	4.1	34.849	2787	34.934	2985
H7	3.3	34.892	2989	34.928	3097
H8	4.7	34.877	2928	34.934	3239
H9	3.5	34.884	3045	34.929	2765
H10	8.6	34.896	3603	34.950	2213
H11	7.7	34.895	3133	34.938	3354
H12	5.5	34.874	3647	34.911	3419
H13	5.6	34.886	3594	34.911	3511

Note: Inshore station in section H7 taken 3 weeks before remainder of section.

an unknown combination of additional entrainment on the entry to the drift area and geographical variation in reference level velocity to explain the increase in transport. Similarly, the reduction in transport between the drift and the Labrador Basin (between transects D2 and D3 and between H10 and H11) could be due to a combination of reference-level variability and deeper elements of the current crossing the Labrador Basin to the south of sections D3/H11. The drift sections (D2—3614 m and H10—3750 m) extend to greater depths than their Labrador Sea equivalents (D3—3498 m and H11—3442 m). As the current is seen to extend beyond the 3500 m isobath on the drift sections, a fall in actual DWBC transport at the Labrador Basin sections is to be expected.

Of the other historical sections, H2–H7 lie very close to D1 while H8 and H9 reside only slightly further to the south (Fig. 4a). These historical sections show baroclinic transports that are similar to that of D1 (3.3–5.1 Sv). The two historic Labrador Basin sections (H12 and 13) show slightly higher than average transports but not to the extent of the 1962 and 2005 sections, even though they extend to slightly greater depths (3573 and 3594 m). These two sections were taken in May 1994 and May 1997, and the closest Irminger Basin section is H5, occupied in November 1994. Therefore, it is not possible to assess how these transports compare with the DWBC transport in the Irminger Basin at the same time.

Moving on to the internal structure of the current, we can see clearer evidence of multiple cores in the historical data than was present in the Discovery data (Fig. 10). The presence of multiple cores could be explained by variable isopycnal gradients, eddy formation, topographic Rossby waves, or the propagation of multiple strands from the overflows.

The magnitude and position of the maximum and minimum salinities observed within the current (typically in the lower 500 m of the water column for bottom depths greater than 2000 m but with some adjustment on a case by case basis) offer some insight into the relative contributions of ISOW and DSOW (Table 4). The local salinity maximum within the current is typically found near the top of the flow, close to the 500 m height mark corresponding to the highest concentration of ISOW. The local minimum is typically found within 100 m of the bottom in the area of purest DSOW. The position of the salinity minimum on the slope, however, shows some distinct variation.

In the D298 sections, both the salinity minimum and oxygen saturation maximum were found in the slower moving, outer reaches of the current below 3000 m. This appears to be the more typical structure (see Table 4), but section H4 from 1962 provides a distinct contrast, with the salinity minimum much higher up the slope at a bottom depth of 2606 m. A cross-plot of potential temperature versus salinity for this section (Fig. 10—H4)

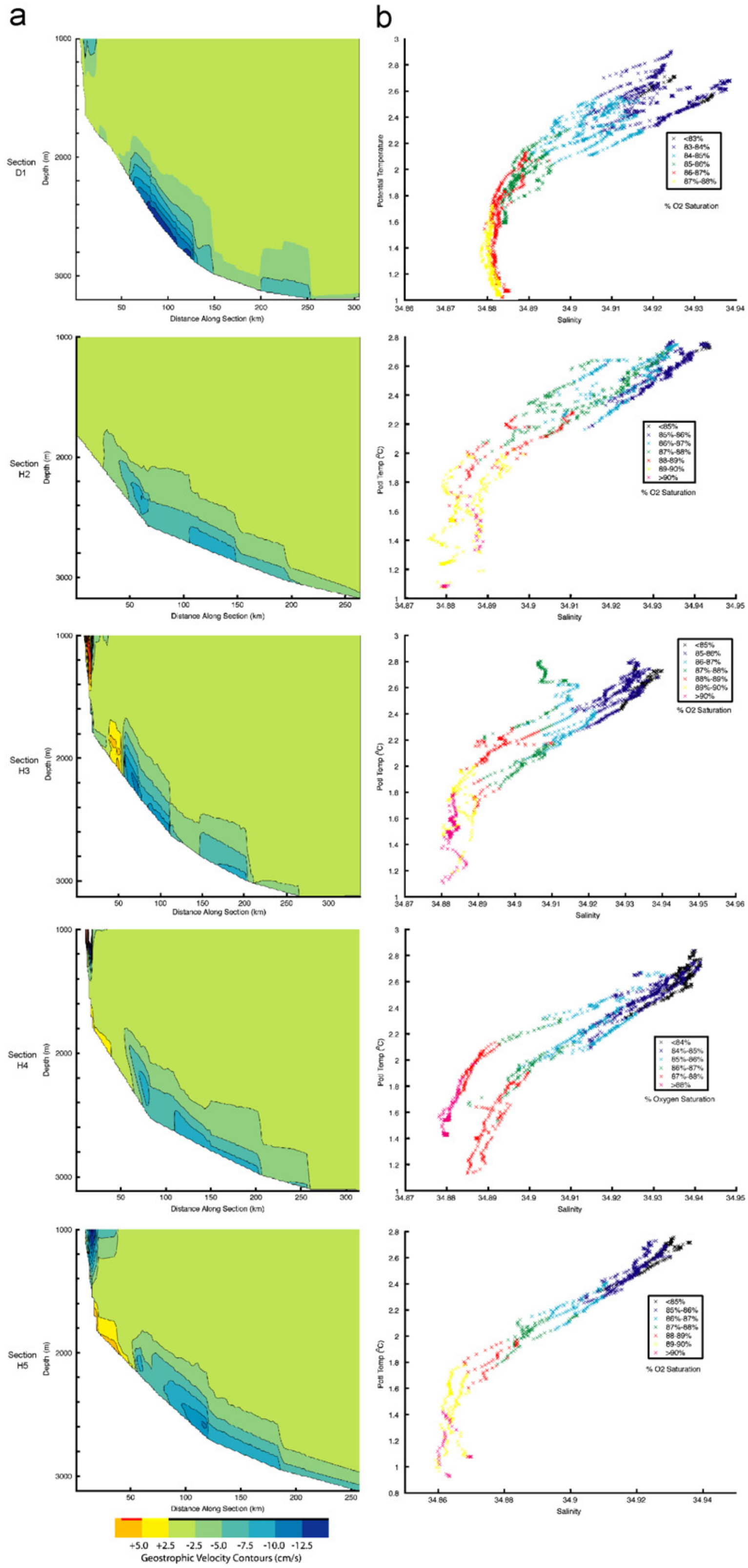

Fig. 10. Comparison of velocity cross-sections and water-mass characteristics between new and historic sections from the same location in the Irminger Sea.

reveals the presence of two mixing lines indicating two distinctly different DSOW end members. The slightly lower salinity branch corresponds to the upper portion of the current with a clearly identifiable separate core. This branch shows higher oxygen saturations, which implies that it has either exited the Denmark Strait more recently, or undergone less mixing with water masses of lower oxygen saturations. The difference in oxygen saturation of about 0.7% between the two branches is similar in magnitude to the range in maximum saturation values between sections D1 and D2 that are separated by about 500 km along the 3000 m isobath, equating to a travel time of about 29 days (with a typical current velocity of 20 cm/s). Even if we allow for some mixing, the observed difference in oxygen saturation between the two strands of the current in section H4 suggests that the age difference between them is of the order of a few months.

The positioning of the younger strand higher up the slope (Fig. 10—H4b) is the result of its higher temperature and suggests that, in at least this case, the multi-core appearance of the current is the result of strand separation at the overflow. Such a temperature-driven shift across the slope would be consistent with the observations of Dickson et al. (1999) but suggests that such variation can occur over much shorter time periods than they may have considered. Fig. 10 (H2, H3 and H5) shows cross-plots and velocity sections for the other historic sections for which oxygen saturation data were available on the WOD. Viewed together these present a range of possible scenarios from primarily single-core currents with single ISOW and DSOW end members (D1 and H5), through two DSOW or ISOW end members with only narrow separation resulting in some mixing (H2 and H3), to the clearly separate current strands with two end DSOW end members (H4). These observations support the hypothesis that high short-term velocity variability seen in current metre records could be driven, in part, by lateral current core movements that do not necessarily have the same impact on overall transport variability.

5. Holocene sedimentation on the Eirik Drift

5.1. Geological data and methods

The main geological resource used in this study is a collection of 3.5 and 5.1 kHz profiler lines acquired in 2003, 2004 and 2005 (Table 5) along with a sidescan sonar line acquired in 2003. The acoustic character, or echo-character types, observed within the profiler sections have been described following the work of Damuth (1975, 1980) and Jacobi and Hayes (1982) in order to assess the different sedimentary regimes within the study area. Four main echo-character types were identified based on the characteristics of the seabed echo and on the presence or absence and character of any sub-bottom echoes (Table 6). As discussed by Bianchi and McCave (2000), the temporal resolution of echo-character data is constrained by the vertical resolution of 3.5 kHz data (around 40 cm) and sedimentation rate, with the time interval that can be resolved of the order of 1–10 ka. Profiler data therefore represent mean conditions over several thousand years so that the extent to which these data represent the modern conditions needs to be carefully assessed. The echo types have therefore been interpreted with reference to the sidescan sonar data, core data and bottom photographs in terms of the relative degree of sedimentation versus erosion or non-deposition they represent and the local hydrographic process likely to be responsible for their development.

Table 5
Sources of 3.5 and 5.1 kHz profiler data

Cruise	Year	Vessel	Data type (kHz)
TTR-13	2003	R.V. *Professor Logachev*	5.1
CD-159	2004	R.R.S. *Charles Darwin*	3.5
D298	2005	R.R.S. *Discovery*	3.5

For a composite section across the drift, the seabed reflector has been picked using ProMAX seismic interpretation software. Analysis of the relative amplitude of the seabed acoustic reflection allows the sedimentary characteristics of the seabed to be estimated, although with a low lateral resolution of the order of several hundred metres (Szuman et al., 2006).

Variations in the intensity of backscatter along sidescan sonar line makat-86 have been interpreted in terms of probable variations in the mean grain size of the surface sediment, in turn reflecting variations in the relative degree of sediment winnowing. Recent studies on continental shelf sediments have shown a strong correlation between the mean grain size of surface sediment and the intensity of acoustic backscatter, with brighter

Table 6
Summary of the echo-character types observed in the Cape Farewell–Eirik Drift region

Type	Description	Interpretation
ET1	Semi-prolonged to prolonged high amplitude seabed echo with few or no sub-bottom echos and smooth to wavy microtopography	High proportion of sand/silt in sediments (Damuth, 1980) Erosional, high-energy conditions
ET2	Sharp, moderate to high amplitude seabed echo with multiple, closely spaced, parallel, continuous low to high amplitude sub-bottom echos. Smooth to wavy micro-topography	Low proportion of sand/silt in sediments (Damuth, 1980) Pelagic/hemipelagic or contourite sedimentation
ET3	Sharp, low amplitude seabed echo underlain by two closely spaced high amplitude sub-bottom echos and two moderate amplitude echos interspersed with a number of low amplitude reflectors Smooth (ET3A) to wavy (ET3B) microtopography	See discussion in text
ET4	High amplitude, hazy reflectors intermittently overlain by a very low amplitude seabed echo	Moderate proportion of sand/silt (Damuth, 1980) Abyssal plain with fine-grained sediment drape

backscatter indicating a larger mean grain size (Goff et al., 2000; Collier and Brown, 2005). Collier and Brown (2005) report a positive correlation with a coefficient of 0.73 between the mean backscatter intensity and the mean surface sediment grain size. As most surface sediments on the upper drift, in the region from which line makat-86 was taken, appear to be winnowed sands, this result is likely to have relevance here. Lineations observed in the sidescan sonar data are considered to reflect current activity (e.g. Kuijpers et al., 2003) and are therefore used as current direction indicators.

To corroborate the backscatter and echo-character interpretations, sedimentological data from the tops of three recently recovered cores (TTR13-AT450G, TTR13-AT451G (hereafter TTR13-450 and 451) and D298-P3) and published bottom photographs (Rabinowitz and Eittreim, 1974) have been used. No evidence of significant loss of surface sediment was observed during the recovery of the cores. The bulk grain size distribution of the upper centimetre of sediment was determined using a Malvern Mastersizer, 2000 laser granulometer and is assumed to be representative of modern sedimentological conditions.

The locations of the newly acquired and published geological and geophysical data used in this study are shown in Fig. 4b.

5.2. *Holocene sedimentary regimes*

The depositional regimes present across the Eirik Drift are mapped on Fig. 11a and discussed in detail below. For comparison, the high and low-velocity zones of the DWBC, as determined from the D298 hydrographic data, are mapped in Fig. 11b along with the region of interpreted high fine sediment load associated with the DSOW and the pathway of the surface, iceberg-bearing East Greenland Current (EGC) (from Holliday et al., 2007). The proportions of clay minerals present in the surface sediment are also shown (from Fagel et al., 1997) as these may be interpreted as a tracer for sediments transported by the DWBC.

The southeastern flank of the main ridge and the southwestern flanks of the upper two secondary ridges above around 2800 m are characterized by a high-amplitude seabed echo that is underlain by a diffuse blackened zone, caused by very high acoustic backscatter, with few or no sub-bottom reflections (Fig. 12a). This echo-character type (ET1) is typical of coarse seabed sediments with a high proportion of sand and silt, resulting from non-depositional or erosional conditions (e.g. Damuth, 1980; Stow et al., 2002). This is confirmed here by the presence of sandy surface sediments in core TTR13-450 and the rocky seabed (from IRD dropstones) recorded in bottom photograph 1 (Fig. 12a). Both the modern and historic hydrographic data show that these upper drift flanks are occupied by the upper portion of the DWBC (Figs. 6, 10 and 11b), where the calculated geostrophic velocities are up to 25 cm s^{-1} (Table 3) and are easily capable of producing the coarse, winnowed surface sediments observed, given an input of mixed size IRD from which the mud is removed.

On the northern flank of the main ridge and northeastern flanks of the upper two secondary

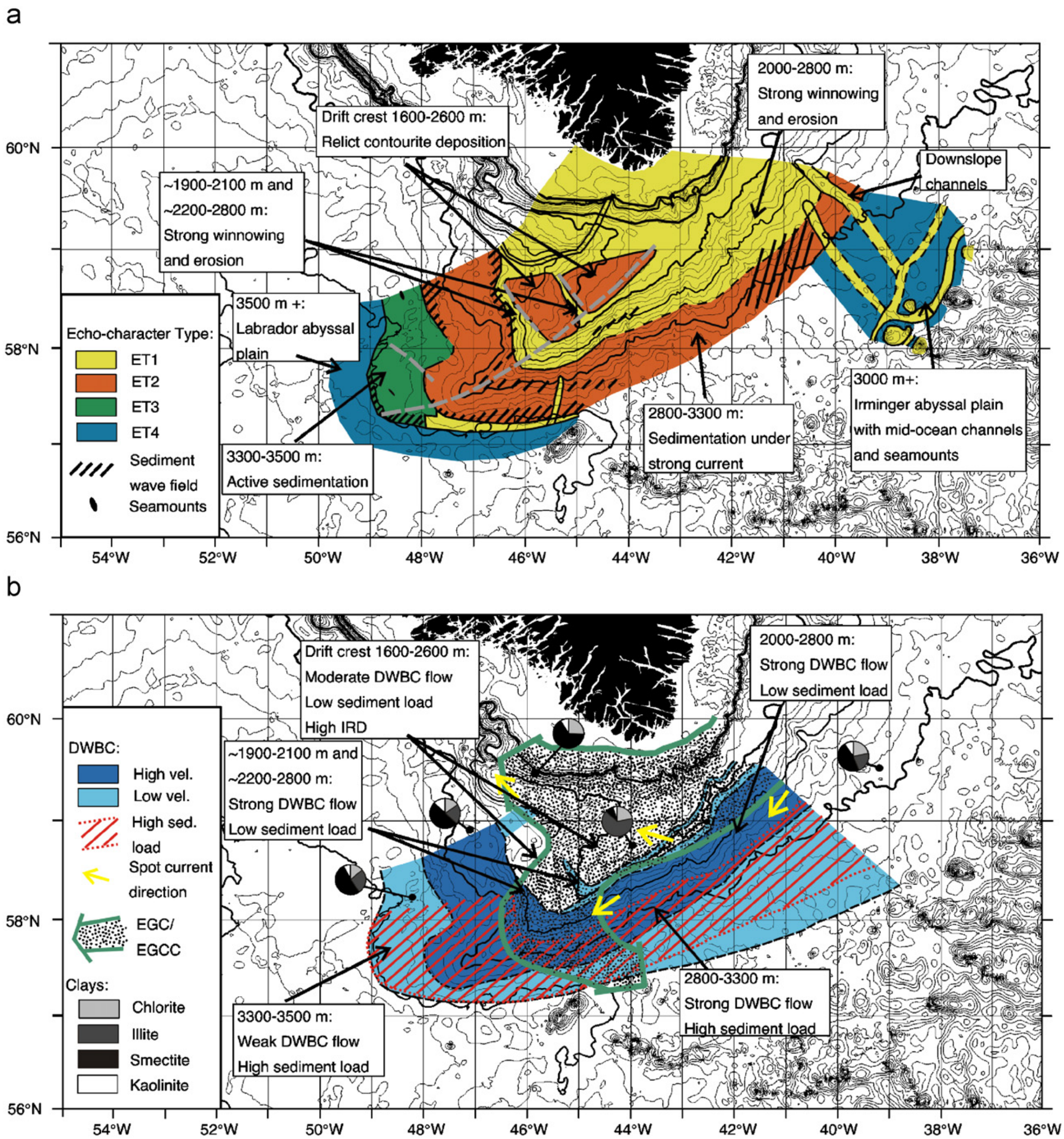

Fig. 11. (a) Spatial distribution of sedimentation regimes determined from echo-character data. The positions of the main and secondary ridge crests are indicated in grey and (b) spatial distribuition of DWBC characteristics determined from the D298 hydrographic data. High-velocity areas indicate calculated geostrophic velocity $>7.5\,\mathrm{cm\,s^{-1}}$ and high sediment load indicates areas with a beam attenuation coefficient $>0.42\,\mathrm{m^{-1}}$. The yellow arrows show the direction of deep current flow, determined from spot current measurements, where the velocity exceeded $20\,\mathrm{cm\,s^{-1}}$ (from Rabinowitz and Eittreim, 1974). The position of the East Greenland Current/East Greenland Coastal Current (EGC/EGCC) is also shown (from Holliday et al., 2007). The pie diagrams show the relative proportions of clay minerals in the surface sediment at various locations across the study area (from Fagel et al., 1996).

ridges, the seabed acoustic reflectivity remains high, but the level of acoustic penetration increases and several parallel, laterally continuous sub-bottom echoes are visible (Fig. 12a). This echo type (ET2) typically characterises depositional environments with a low proportion (0–5%) of coarse sediments

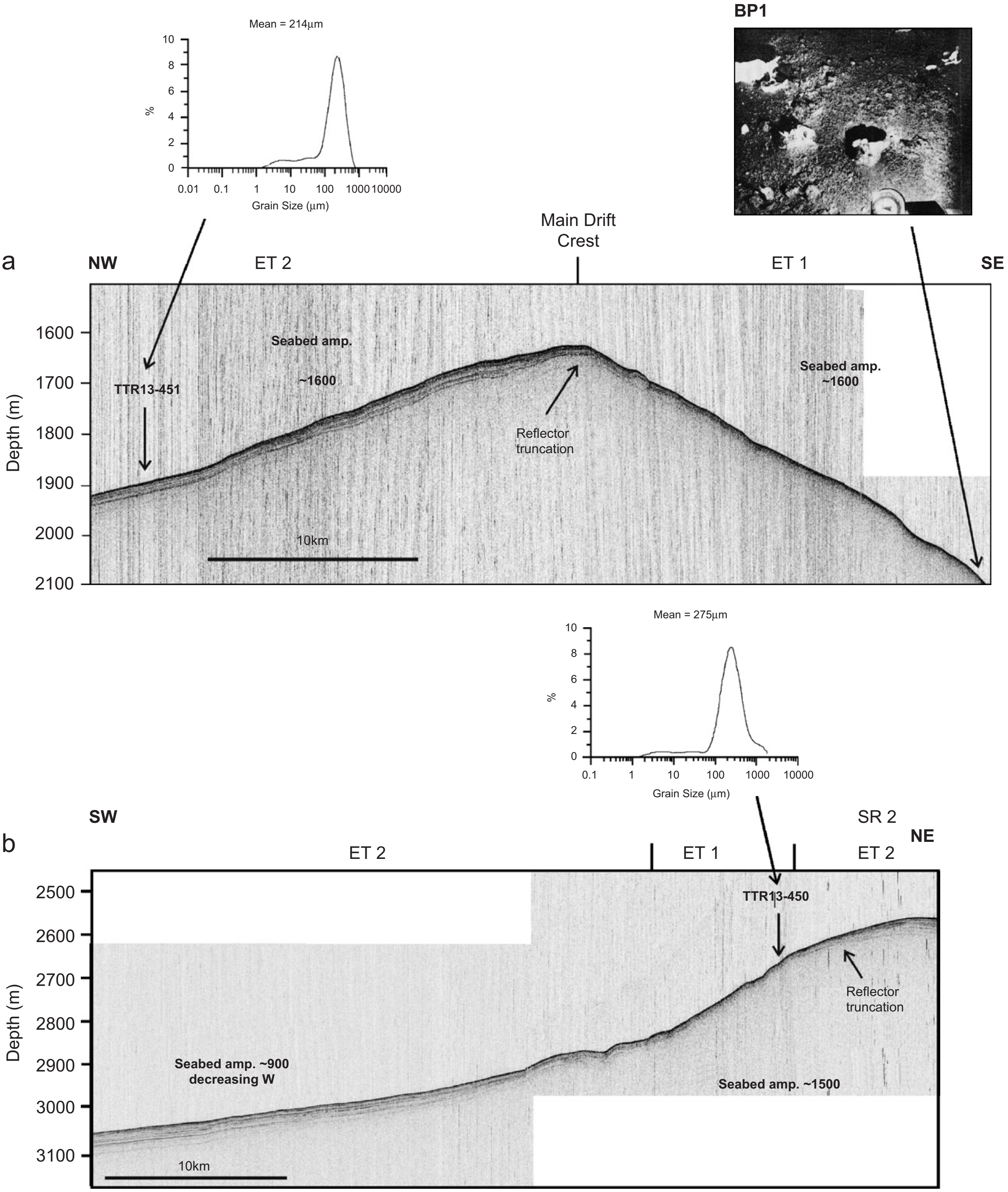

Fig. 12. Echo characteristics of the upper Eirik Drift: (a) drift crest area with the rocky seabed present to the south of the main drift crest shown by bottom photograph 1 (BP1—from Rabinowitz and Eittreim, 1974) and the presence of sandy surface sediments to the north of the crest shown by the grain-size distribution from the surface of core TTR13-451 and (b) section showing the central, most prominent secondary ridge on the northern drift flank, with grain size distribution data from core TTR13-450 close to the upper margin of ET1. The average seabed acoustic reflection amplitude within each of the echo-character zones is also indicated.

(Damuth, 1980) and is commonly interpreted as representing pelagic or hemipelagic sedimentation, although it is also typical of contourite deposition (e.g. Damuth, 1980; Stow et al., 2002).

This spatial pattern of echo type distribution, with ET1 on the steeply sloping drift flanks and ET2 across the crest from the main current pathway (Figs. 11a and b), is also observed on other North Atlantic drifts (e.g. the Bjorn and Gardar Drifts—Bianchi and McCave, 2000) where it is interpreted to represent winnowing and erosion under strong contour currents along the drift flanks with deposition upslope. However at the Eirik Drift, sandy surface sediments are present within the ET2 zone on the upper northern drift flanks (Fig. 12a), suggesting significant winnowing of the fine fraction. This, together with the presence of a condensed Holocene sequence in this area (Stanford et al., 2006), demonstrates that this is not an area of active modern sedimentation. However, the D298 hydrographic data suggest very little current activity in this ET2 zone capable of significant sediment winnowing (Figs. 6 and 11b). As discussed in Section 4.3, the geostrophic velocity observed in section D2 in the vicinity of the drift crest may be an underestimation of the actual velocity and spot current measurement data show flow of in excess of 20 cm s^{-1} across the drift crest (Fig. 11b).

Beam attenuance data from the D298 hydrographic sections show that the DWBC carries very little sediment above around 2800 m (Figs. 6d and 11b), indicating a low lateral sediment input to both the ET1 and 2 zones above this depth. The surface and intermediate waters overlying these upper drift flanks are however occupied by the EGC (Fig. 11b), which as a major conduit for icebergs will provide a supply of IRD to this area. This IRD, along with biogenic inputs, forms the only significant source of sediment to the upper drift flanks. The sandy surface sediments observed in both the ET1 and ET2 zones on the upper drift flanks are therefore interpreted to result primarily from the winnowing of these ice-rafted and biogenic sediments, yielding slow sedimentation of a sand-dominated sequence. The relative abundance of clay minerals in the surface sediments from within both of these zones shows a high proportion of illite (Fagel et al., 1997) (Fig. 11b), which would appear to be a result of this ice-rafted origin.

Sub-bottom reflectors within this ET2 zone are parallel with respect to the seabed and lack obvious truncation, suggesting no significant down-cutting. It seems therefore that the area to the north of the drift crest has been dominantly non-depositional throughout the Holocene, with sediment re-working and winnowing. At the margins of the ET2 zones, however, downward truncation of the sub-bottom reflectors toward ET1 zones (Fig. 12) suggests a progressively increasing degree of erosion toward the high-velocity current cores.

The presence of secondary ridges to the north of the main ridge crest, each with associated zones of ET1 and ET2 (Fig. 11a), suggests the presence of separate DWBC strands in this area. The erosive ET1 zone on the southwest flank of the central secondary ridge occurs at around 2200–2800 m (Fig. 11a) and is associated with the upper part of the main DWBC core (Fig. 11b). The upper, minor ridge displays an erosive area between 1900 and 2200 m (Fig. 11a). A small, detached strand of contour-flowing current is observed at this depth in both the D298 and historic geostrophic velocity data (Figs. 6, 10 and 11b), and water mass characteristics suggest that this is most likely a separated strand of the DWBC (Fig. 6b and c). The depth of this current strand is consistent with the flow of North East Atlantic Deep Water 1 (upper ISOW) through the Bight Fracture Zone in the Reykjanes Ridge, described by Lucotte and Hillaire-Marcel (1994).

Sidescan sonar line makat-86 crosses areas of both ET1 and 2 in the vicinity of the main ridge crest (Fig. 13), allowing further interpretation of the sedimentary processes in these zones. A relatively high degree of backscatter and a featureless surface texture characterise the ET1 zone on the south-eastern flank of the drift, while on the northwestern flank, the ET2 zone shows a somewhat lower degree of backscatter and displays distinct surface lineations. The higher backscatter to the southeast of the main drift crest is consistent with the somewhat higher mean grain size observed in this area (Fig. 12) and with bottom photographs from within this zone (Fig. 12b) that show a rocky seabed with a lack of fine-grained sediments (Rabinowitz and Eittreim, 1974). The observed surface lineations to the north of the drift crest include 'comet-tail' features with high backscatter tails extending up to 100 m to the north and northwest from blocky features a few metres in diameter (Fig. 13). These are interpreted to represent coarse lag deposits extending downstream from large glacial boulders similar to those seen in bottom photographs from the Newfoundland Margin (Carter and Schafer,

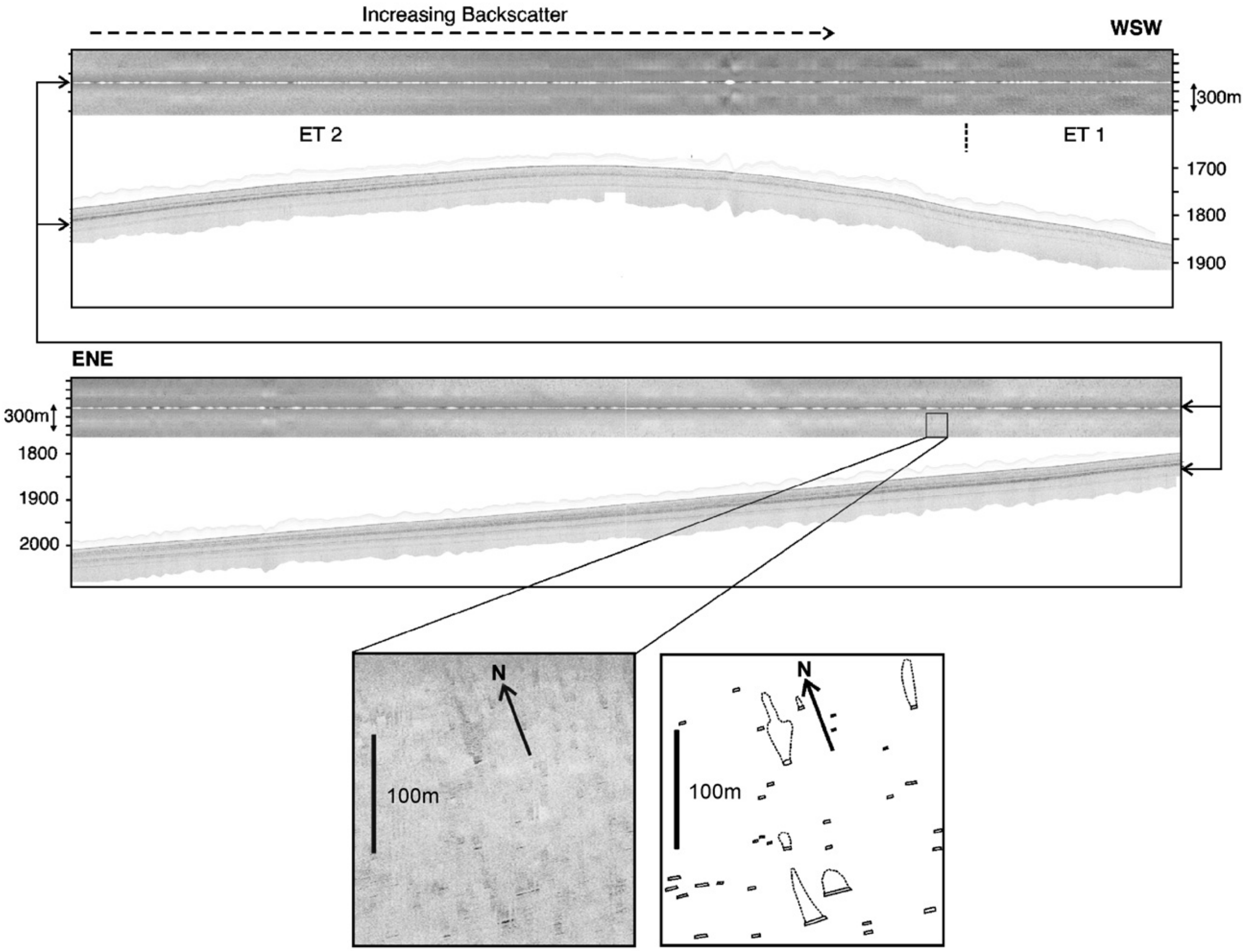

Fig. 13. Sidescan sonar line crossing the drift crest, with the corresponding 3.5 kHz section shown below (location shown on Fig. 4b). The inset shows the detailed surface texture within the ET2 zone on the northern drift flank, with comet-tail features, highlighted in the adjacent line drawing, indicating unidirectional flow.

1983), indicating unidirectional flow. The orientation indicates flow to the north and northwest suggesting flow across the drift crest and supports the inference of significant flow across the drift crest based on the spot current measurement data.

On the lower drift flanks, below about 2800 m, sub-bottom echoes become visible once more (ET2), suggesting that these areas are, or have been, depositional (Figs. 12b and 14). Published core data from just below 2800 m on the northern drift flank shows the presence of sandy sediments throughout the Holocene with 30–40% of the bulk sediment greater than 125 μm (Hillaire-Marcel et al., 1994). However, bottom photograph 2 from the upper part of this zone on the southeastern flank of the main ridge (Fig. 14) indicates the presence of fine-grained sediments at the seabed (Rabinowitz and Eittreim, 1974) suggesting ongoing deposition. The seabed acoustic reflection amplitude is somewhat lower here than in the ET2 zone above 2800 m (Figs. 12a and b), most likely as a result of finer and less dense surface sediments. Bottom photograph 2 also shows surface lineations indicating a strong current influence, which is also suggested by the pervasive occurrence of low amplitude, symmetrical sediment waves (Figs. 11 and 14). The hydrographic data show high DWBC flow velocities in this depth interval, comparable to those within the erosive ET1 zone on the upper drift flanks (Figs. 6, 10 and 11b).

The above identifies a marked difference in the character of surface sediment between the lower and upper drift flanks, despite the similar flow velocities observed over these areas. The lower, more depositional drift flanks corresponds with the region of

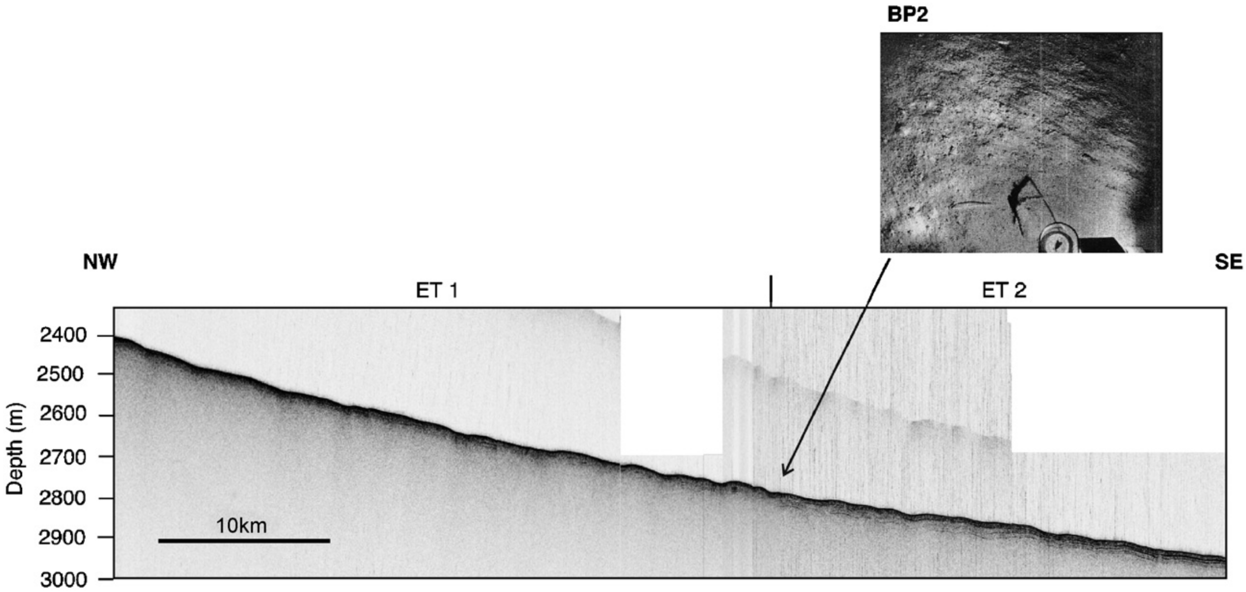

Fig. 14. Echo characteristics of the deep-water, southeastern flank of the Eirik Drift, with fine surface sediments in the deep ET2 zone shown by bottom photograph 2 (BP2—from Rabinowitz and Eittreim, 1974).

high oxygen saturation, high beam attenuation and low salinity that represent the sediment-laden DSOW within the D298 hydrographic sections (Figs. 6 and 11b). The surface sediment clay mineral data also show the presence of a high proportion of smectites within this lower ET2 zone on both the southern and northern drift flanks, linked to sediment transport by the DSOW (Fagel et al., 1997). On the upper drift flanks, however, the only significant sediment sources are IRD and biogenic input. The degree of surface sedimentation associated with the DWBC at the Eirik Drift appears therefore to be controlled by the availability of an abundant lateral sediment supply, rather than by flow velocity alone.

The deep-water drift toe at the base of the northern drift flank is characterised by a distinctive echo-character type (ET3) that consists of a low to moderate amplitude seabed echo underlain by two closely spaced, high amplitude sub-bottom echoes and two moderate amplitude echoes, interspersed with a number of low amplitude reflectors (Figs. 11a and 15).

The upper prominent reflector occurs at approximately 5.5 m below the seafloor in the vicinity of core D298-P2 (depth calculated based on the average p-wave velocity of 1454 m s^{-1} measured in core D298-P2). This depth closely corresponds with the upper boundary of sediments bearing ice rafted debris (IRD) (Fig. 16). Comparison of the magnetic susceptibility record with a nearby published, radiocarbon dated record shows this boundary to represent the base of the Holocene (Stoner et al., 1995). The upper transparent unit lying above this reflector is therefore interpreted as the Holocene sequence. The thickness of this sequence, up to 12 m in places, shows that this deep-water area has experienced very active sedimentation at rates of 50–100 cm ka^{-1}. Surface sediments from core D298-P3, from the north of this depositional area, are composed primarily of silt and clay (Fig. 15), indicating an environment dominated by the accumulation of fine sediments, suggesting that the active sedimentation in this area continues to the present day.

Moderate to high amplitude discontinuous sub-bottom echoes are observed within the Holocene unit that have a lateral extent of up to 10 km. These discontinuous echoes correspond closely in depth with the thickest and most prominent of the turbidites in core D298-P2 (Fig. 16) and are therefore interpreted throughout the study area as turbidites.

Hydrographic data show this deep-water region, between 3300 and 3500 m on the northern drift flank, to be characterised by low DWBC velocities with an intense bottom nepheloid layer within the DSOW-dominated lower part of the current

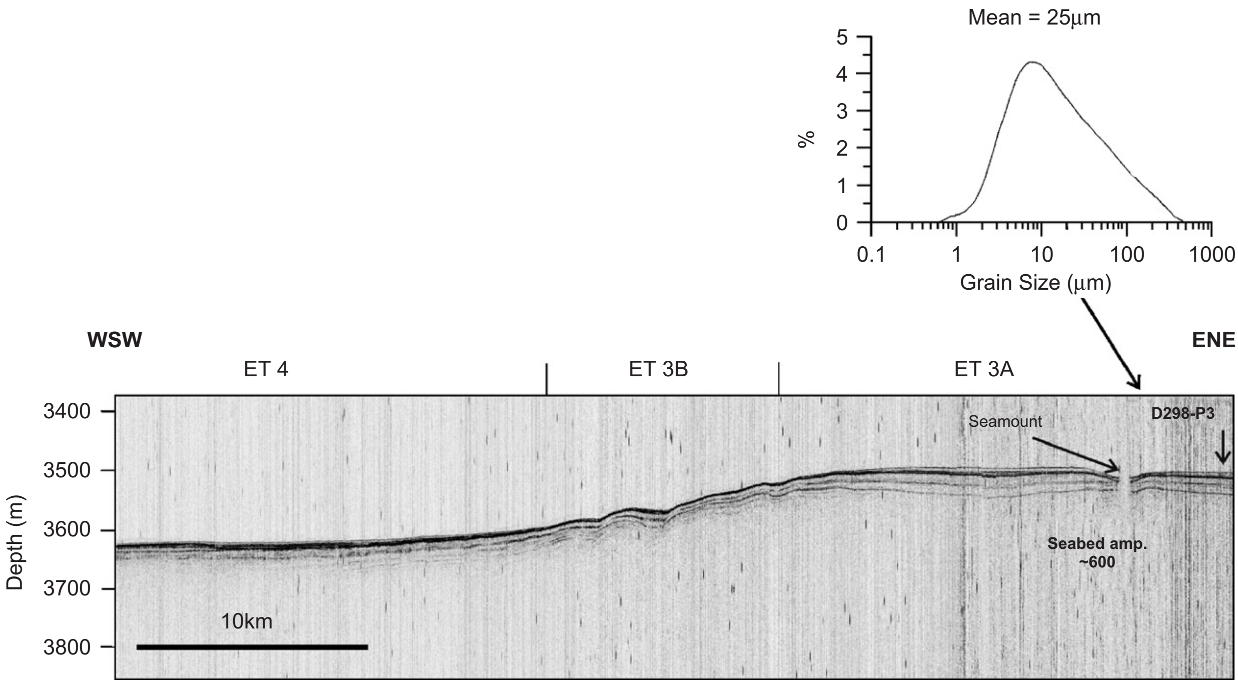

Fig. 15. Echo characteristics of the deep-water western drift toe and Labrador abyssal plain, with grain size distribution data from core D298-P3.

(Fig. 6). Surface clay mineral data also show this area to have a high component of smectites, typical of DSOW-influenced deposition (Fagel et al., 1997) (Fig. 11b). A combination of low current velocities and abundant lateral sediment supply are therefore the most likely cause of the rapid sedimentation observed in this area. The fact that a thick Holocene sequence is seen only in profiler data from the north of the drift crest indicates that deceleration of the DWBC as it rounds the drift initiates this enhanced deposition.

The abyssal plains of both the Irminger and Labrador Basins are characterised by high amplitude, hazy reflectors that are intermittently overlain by a very low amplitude seabed echo (Fig. 15). This echo type (ET4) is interpreted as representing sediments that contain a moderate amount of sand and silt (0–30%—Damuth, 1980), intermittently overlain by a thin drape of fine-grained sediments. The very offshore end of hydrographic section D1 shows the low-velocity margin of the DWBC extending out into the centre of the Irminger Basin (Fig. 6). The low velocity and moderate sediment load associated with this current margin appear to have allowed limited recent deposition to extend toward the basin centres.

6. Discussion and conclusions

The Holocene sediment record from the Eirik Drift indicates that recent sedimentation has only occurred down slope of the main DWBC, at the foot of the continental slope. Modern hydrographic data show this to be an area where the current typically has the highest proportion of sediment-laden DSOW. This sediment load can be deposited as the current rounds the drift. However, even recent hydrographic data indicate that the structure of the DWBC can vary with warmer current cores of DSOW appearing higher up the drift flanks (Fig. 10). Although we would expect such a DSOW core to carry sediment loads capable of deposition, the lack of significant Holocene sedimentation higher up the slope tells us that this can only have been an occasional feature in recent times.

The lack of sedimentation on the drift crest during the Holocene raises the question of the differences between this period and earlier phases of drift construction during the Pliocene and Pleistocene when sediment accumulation did occur on the drift crest. Significant sediment accumulation during glacial phases of the Pleistocene has been linked to limited current activity (Hillaire-Marcel et al.,

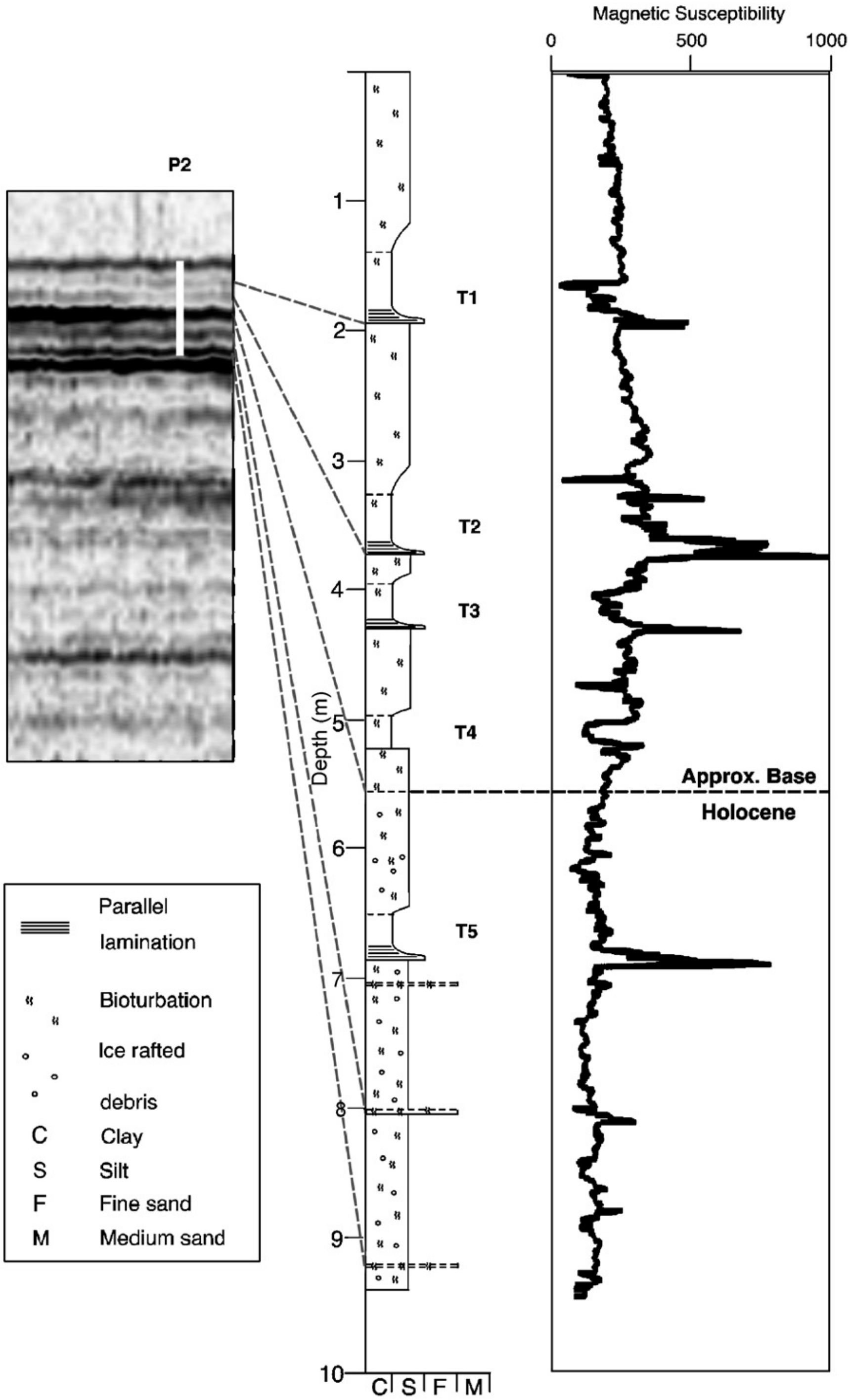

Fig. 16. A 3.5 kHz section from the vicinity of core D298-P2 along with the core log and magnetic susceptibility record from D298-P2 showing the probable origin of the observed sub-bottom echoes. T1–T5 = Turbidites 1–5.

1994). The Pliocene, however, was characterized by strong DWBC flow in this area (Arthur et al., 1989). Seismic sections show the Pliocene sequence of the drift with pervasive sediment waves and the formation of strongly migrating drift crests that have led to the present drift morphology (Srivastava et al., 1989; Hunter et al., 2007). The most obvious reason for the difference between the Pliocene and

Holocene intervals therefore would be a higher sediment supply during the Pliocene, which has been inferred from widespread drift building in the region and may have resulted from local uplift along the Greenland–Scotland Ridge (Wold, 1994). The sequence of drifts found along the path of ISOW, from the Bjorn Drift (Miocene-Quaternary) in the Iceland Basin to the Gloria Drift (Pliocene-Quaternary) in the southern Irminger Basin, suggests that the sediment load carried by the DWBC over the Eirik Drift during this period may have been supplied by a combination of DSOW and ISOW.

Whilst DSOW flows directly from the sill at Denmark Strait to its first major turning point off Cape Farewell, the path of ISOW is more complex. In addition to navigating the bathymetry of the Iceland Basin (resulting in the formation of the Bjorn and Gardar Drifts—Fig. 17), it can follow a number of routes between exiting the Iceland Basin and joining the main DWBC. The normally documented route sees ISOW following bottom contours of less than ca. 3000 m from the CGFZ around the Irminger Basin to a confluence with the DSOW driven DWBC to the north of the Eirik Drift. However, the water mass tracer data discussed here support the hypothesis that deeper components of the ISOW/LDW combination flowing out of the CGFZ at depths below 3200 m follow the bathymetry across the Irminger Basin without passing through hydrographic sections set to the south-east from Cape Farewell (Fig. 17a) (McCartney, 1992). Lherminier et al. (2007) identify two cores of ISOW flowing south along the south-eastern flanks of the Reykjanes Ridge marked by locally elevated oxygen concentrations. The deeper core is at a depth of around 3500 m in the Maury Channel and has an elevated silicate concentration in excess of 15 μmol/kg. This deep silicate maximum at the foot of the Rekyjanes Ridge has been previously identified further north in the Iceland Basin by Mann et al. (1973). Although Lherminier et al. (2007) suggest that this deeper strand is in part due to an Icelandic Basin recirculation, its depth and silicate content is consistent with our hypothesis of a deeper, more LDW rich, component of ISOW flowing through the deeper reaches of the CGFZ and joining the DWBC well to the south of Cape Farewell.

Transports have been calculated for the overflow water travelling north along the western side of the Reykjanes Ridge based upon data collected by the *Erika Dan* in early 1962 and corresponding to our sections H1, H10 and H11 (Worthington and Volkman, 1965). These show a reduction in the transport from 7.6 Sv at a latitude of 53°30′N to 2.0 Sv at 59°30′N. The maximum depths in the Irminger Basin at these latitudes are ca. 3600 and 3100 m, respectively, and the fall in transport corresponds to the increase we calculate on the other side of the Irminger Basin of 3.5 Sv between sections H1 and H10. Although Saunders (1994) suggests that the reference levels used by Worthington and Volkman (1965) result in an overestimate of the outflow from the CGFZ, these results still provide some support for the hypothesis that the modified ISOW follows different, depth dependent, pathways on exiting the CGFZ according to its potential density relative to the deep/bottom water it encounters in the Irminger Basin. Current metre data presented by Saunders (1994) show a significant westward current flowing through the CGFZ at around 3000 m in the northern channel but without the vertical resolution to identify the flow between 3200 and 3500 m. Bottom currents above about 3200 m on the western flank of the Reykjanes Ridge will flow north into the Irminger Basin before turning south and joining the DWBC upstream of the Eirik Drift (Fig. 17a). Between about 3200 and 3500 m, the expected flow will first cross the Gloria Drift and then join the DWBC on the Eirik Drift. For flow below about 3500 m, the expected route would be across the southern edge of the Gloria Drift, around the mouth of the Labrador Basin, joining the DWBC off Newfoundland without reaching as far North as the Eirik Drift.

The new silicate concentration data collected during cruise D298 show a very similar pattern to those published by McCartney (1992). McCartney's contour map of the deep silicate maximum (Fig. 17b) can be interpreted as showing the pathways of ISOW where the silicate maximum is at the bottom. The point at which the silicate maximum lifts away from the bottom as it is undercut by the denser DSOW marks the offshore extent of the DWBC. This suggests that the deepest component of ISOW barely reaches any of the D298 sections and provides support for the pathway suggested by McCave and Tucholke (1986) for ISOW forming the Gloria Drift to the south of the Eirik Drift.

The separate strand of current identified at around 2000 m in both the D298 and historical hydrographic data is consistent with flow of upper

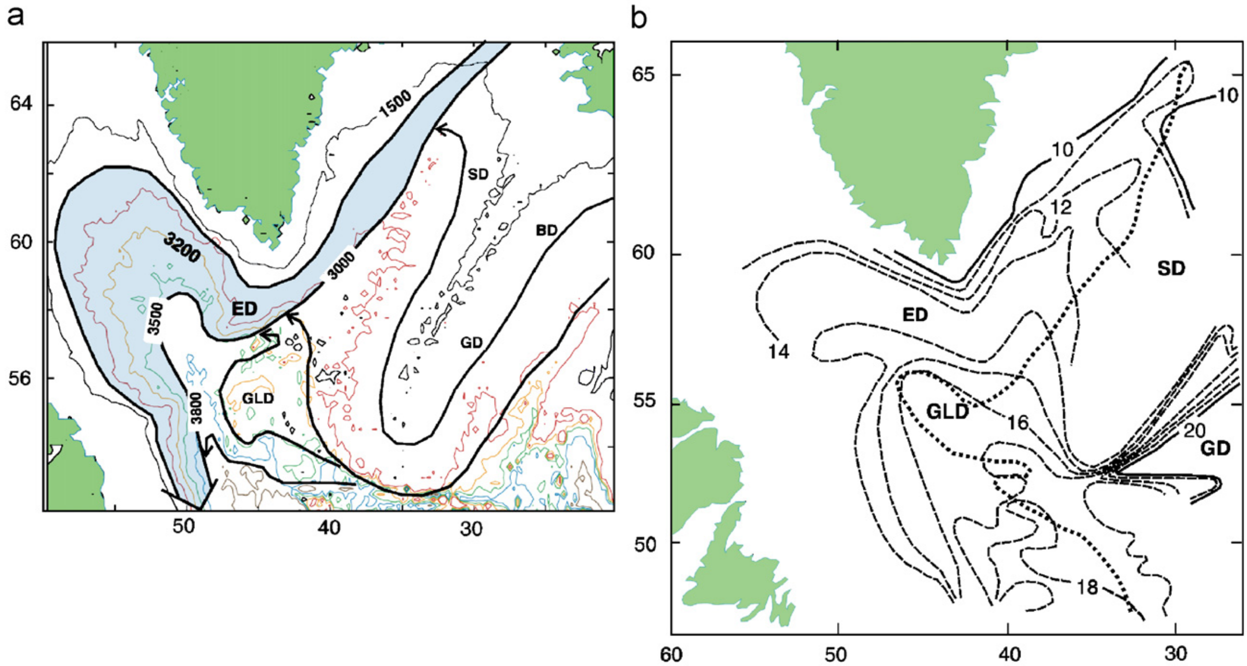

Fig. 17. (a) Schematic representation of the path of the DWBC through the Irminger and Labrador Basins (in blue) with the potential routes by which the ISOW/LDW may join the main DWBC (black arrows) and (b) silicate (μmol l^{-1}) of the deep silicate maximum. This occurs above the bottom to the left of the dotted curve and at the bottom to the right of the curve (from McCartney, 1992). ED, Eirik Drift; GLD, Gloria Drift; SD, Snorri Drift; GD, Gardar Drift; BD, Bjorn Drift.

ISOW through the Bight Fracture Zone in the Reykjanes Ridge (Lucotte and Hillaire-Marcel, 1994) and overlies the southwestern flank of the upper secondary ridge on the northern flank of the Eirik Drift. It has been postulated that the formation of the secondary ridges on the Eirik Drift relates to basement structure (Hunter et al., 2007). However, the coincidence between the location of the upper ridge and a strand of current that is clearly identifiable along the southeast Greenland margin, before any possible influence of local structure at the drift, suggests that the multi-cored nature of the DWBC in this region may also have played a role in the development of the ridges.

The area bounded by Cape Farewell to the north, the CGFZ to the south-east and Newfoundland to the south-west contains a complex combination of interacting deep currents. By the time the DWBC reaches Newfoundland it has been joined by the majority of the modified ISOW flowing through the CGFZ and its transport is a good indicator of the strength of the global THC. However, the growth in the DWBC transport as it flows around the Eirik Drift is significantly affected by the proportion of ISOW flowing along the different depth/density controlled pathways discussed earlier. The cross-sectional structure of the current will also be affected by the relative densities and water characteristics of the two types of overflow water and the overlying LSW.

We have illustrated how the DSOW core(s) flowing down the Greenland margin can move significantly across the slope over timescales of months (as seen in the hydrographic data from the WOD) and years (Dickson et al., 1999) as a result of temperature changes in the surface waters of the Arctic. Similar variations in the ISOW could alter the proportion of water following the different depth-controlled pathways providing a source of short-term variability in the transport of the DWBC over the Eirik Drift and affecting its cross-sectional structure. Some variability in the relative density of ISOW, LSW and DSOW is to be expected as the difference in their travel times from their area of formation to the Cape Farewell region means that the combining flows are sourced from mode waters of different ages.

In conclusion, the transport of the DWBC around the Eirik Drift and the rate of sedimentation in individual locations can be affected by changes in the overflow waters that do not necessarily impact the overall strength of the DWBC as it exits the Labrador Basin and feeds the lower limb of the THC. Although sedimentation patterns reflect average current pathways, even over longer periods, the potentially complex behaviour of the DWBC needs to be considered in the interpretation of paleo-DWBC proxy records from sediment cores.

Acknowledgements

This study was funded as part of the NERC Rapid Climate Change Program under Grants NER/T/S/2002/00453 and NER/T/S/2002/00436. The authors wish to thank all those associated with cruises D298, CD159 and TTR-13. The TTR-13 cruise was organised as part of the UNESCO Training Through Research program. The assistance of Dr Simon Dean in the processing of the 3.5 kHz data is also gratefully acknowledged. The cores used in this study are stored at BOSCORF at the National Oceanography Centre, Southampton.

References

Alvarez, M., Perez, F.F., Bryden, H., Rios, A.F., 2004. Physical and biogeochemical transports in the North Atlantic subpolar gyre. Journal of Geophysical Research 109 (C03027).

Arthur, M., Srivastava, S. P., Kaminski, M., Jarrard, R., Osler, J., 1989. Seismic stratigraphy and history of deep circulation and sediment drift development in the Baffin Bay and the Labrador Sea. In: Srivastava, S.P., Arthur, M., Clement, B., et al. (Eds.), Proceedings of the Ocean Drilling Program, Scientific Results, vol. 105, Ocean Drilling Program, College Station, TX, pp. 957–88.

Bacon, S., 1997. Circulation and fluxes in the North Atlantic between Greenland and Ireland. Journal of Physical Oceanography 27, 1420–1435.

Bacon, S., 1998. Decadal variability in the outflow from the Nordic Seas to the deep Atlantic Ocean. Nature 394, 871–874.

Bacon, S., 2006. RRS Discovery Cruise 298, 23 August–25 September 2005. Cape Farewell and Eirik Ridge (CFER-1). Cruise Report No. 10, National Oceanography Centre, Southmapton, 113pp.

Bacon, S., Gould, W.J., Jia, Y., 2003. Open-ocean convection in the Irminger Sea. Geophysical Research Letters 30 (5), 1246.

Bianchi, G.C., McCave, I.N., 1999. Holocene periodicity in North Atlantic climate and deep-ocean flow south of Iceland. Nature 397, 515–517.

Bianchi, G.G., McCave, I.N., 2000. Hydrography and sedimentation under the deep western boundary current on Bjorn and Gardar Drifts, Iceland Basin. Marine Geology 165, 137–169.

Broecker, W.S., 1991. The great ocean conveyor. Oceanography 4 (2), 79–89.

Broecker, W.S., 2000. Abrupt climate change: causal constraints provided by the paleoclimate record. Earth Science Reviews 51, 137–154.

Broecker, W.S., Peteet, D.M., Rind, D., 1985. Does the ocean-atmosphere have more than one stable mode of operation? Nature 315, 21–26.

Carter, L., Schafer, C.T., 1983. Interaction of the Western Boundary Undercurrent with the contintal margin off Newfoundland. Sedimentology 30, 751–768.

Chamberlin, T.C., 1906. On a possbile reversal of deep-sea circulation and its influence on geologic climates. Journal of Geology 14, 363–373.

Clarke, R.A., 1984. Transport through the Cape Farewell Flemish Cap section. Rapport et Proces-verbaux des Reunions, Conseil international pour I'Exploration de la Mer 185, 120–130.

Collier, J.S., Brown, C.J., 2005. Correlation of sidescan backscatter with grain size distribution of surficial seabed sediments. Marine Geology 214, 431–449.

Conkright, M.E., Antonov, J.I., Baranova, O., Boyer, T.P., Garcia, H.E., Gelfeld, R., Johnson, D., Locarnini, R.A., Murphy, P.P., O'Brien, T.D., Smolyar, I., 2002. World Ocean Database 2001, vol. 1: Introduction. US Government Printing Office, Washington, DC.

Damuth, J.E., 1975. Echo character of the western equatorial Atlantic floor and its relationship to the dispersal and distribution of terrigenous sediments. Marine Geology 18, 17–45.

Damuth, J.E., 1980. Use of high-frequency (3.5–12 kHz) echograms in the study of near-bottom sedimentation processes in the deep sea: a review. Marine Geology 38, 51–75.

Dickson, B., Meincke, J., Vassie, I., Jungclaus, J., Osterhus, S., 1999. Possible predictivity in overflow from the Denmark Strait. Nature 397, 243–246.

Dickson, B., Yashayaev, I., Meincke, J., Turrell, B., Dye, S., Holfort, J., 2002. Rapid freshening of the deep North Atlantic Ocean over the past four decades. Nature 416, 832–837.

Dickson, R.R., Brown, J., 1994. The production of North Atlantic Deep Water: sources rates and pathways. Journal of Geophysical Research 99 (C6), 12319–12341.

Eden, C., Willebrand, J., 2001. Mechanism of interannual to decadal variability of the North Atlantic circulation. Journal of Climate 14, 2266–2280.

Fagel, N., Robert, C., Hillaire-Marcel, C., 1996. Clay mineral signature of the NW Atlantic Boundary Undercurrent. Marine Geology 130 (1, 2), 19–28.

Fagel, N., Hillaire-Marcel, C., Robert, C., 1997. Changes in Western Boundary Undercurrent outflow since the Last Glacial Maximum, from smectite/illite ratios in deep Labrador Sea sediments. Paleoceanography 12 (1), 79–96.

Fiadeiro, M.E., Veronis, G., 1983. Circulation and heat flux in the Bermuda Triangle. Journal of Physical Oceanography 13, 1158–1169.

Ganachaud, A., Wunsch, C., 2000. Improved estimates of the global ocean circulation, heat transport and mixing from hydrographic data. Nature 408, 453–457.

Gardner, W.D., Biscaye, P.E., Zaneveld, J.R.V., Richardson, M.J., 1985. Calibration and comparison of the LDGO nephelometer and the OSU transmissometer on the Nova Scotian Rise. Marine Geology 66, 323–344.

Goff, J.A., Olson, H.C., Duncan, C.S., 2000. Correlation of side-scan backscatter intensity with grain-size distribution of shelf sediments, New Jersey margin. Geo-Marine Letters 20, 43–49.

Gross, T.F., Williams, A.J., 1991. Characterisation of deep-sea storms. Marine Geology 99, 281–301.

Hillaire-Marcel, C., de Vernal, A., Bilodeau, G., Wu, G., 1994. Isotope stratigraphy, sedimentation rates, deep circulation and carbonate events in the Labrador Sea during the last ~200 ka. Canadian Journal of Earth Sciences 31, 63–89.

Hiscott, R.N., Cremer, M., Aksu, A.E., 1989. Evidence from sedimentary structures for processes of sediment transport and deposition during the post-Miocene time at sites 645, 646 and 647, Baffin Bay and the Labrador Sea. In: Srivastava, S.P., Arthur, M., Clement, B., et al. (Eds.), Proceedings of the Ocean Drilling Program, Scientific Results, Ocean Drilling Program, vol. 105, College Station, TX, pp. 53–63.

Holliday, N.P., Meyer, A., Bacon, S., Alderson, S.G., de Cuevas, B., 2007. Retroflection of part of the east Greenland current at Cape Farewell. Geophysical Research Letters 34 (L07609).

Hollister, C.D., McCave, I.N., 1984. Sedimentation under deep-sea storms. Nature 309, 220–225.

Hunter, S.E., Wilkinson, D., Stow, D.A.V., Bacon, S., Rohling, E.J., Stanford, J., Kenyon, N.H., Akhmetzhanov, A., 2007. The Eirik Drift: a longterm barometer of North Atlantic Deep Water flux south of Cape Farewell, Greenland. In: Viana, A., Rebesco, M.L. (Eds.), Economic and Paleoceanographic Significance of Contourite Deposits. Geological Society. Special Publication, vol. 276, pp. 245–264.

Innocent, C., Fagel, N., Stevenson, R.K., Hillaire-Marcel, C., 1997. Sm-Nd signature of the modern and late Quaternary sediments from the northwest North Atlantic: implications for deep current changes since the last glacial maximum. Earth and Planetary Science Letters 146, 607–625.

Jacobi, R.D., Hayes, D.E., 1982. Bathymetry, microphysiography and reflectivity characteristics of the West Aftican margin between Sierra Leone and Mauritania. In: von Rad, U., Hinz, K., Sarnthein, M., et al. (Eds.), Geology of the Northwest African Continental Margin. Springer, Berlin, pp. 182–212.

Johnson, L.G., Schneider, E.D., 1969. Depositional ridges in the North Atlantic. Earth and Planetary Science Letters 6 (6), 416–422.

Jones, E.J.W., Ewing, M., Ewing, J.I., Eittreim, S.L., 1970. Influences of Norwegian Sea Overflow Water on sedimentation in the northern North Atlantic and Labrador Seas. Journal of Geophysical Research 75, 1655–1680.

Kuijpers, A., Troelstra, S.R., Prins, M.A., Linthout, K., Akhmetzhanov, A., Bouryak, S., Bachmann, M.F., Lassen, S., Rasmussen, S., Jensen, J.B., 2003. Late Quaternary sedimentary processes and ocean circulation changes at the southeast Greenland margin. Marine Geology 195 (1–4), 109–129.

Lazier, J., Hendry, R., Clarke, A., Yashayaev, I., Rhines, P., 2002. Convection and restratification in the Labrador Sea, 1999–2000. Deep-Sea Research I 49 (10), 1819–1835.

Lherminier, P., Mercier, H., Gourcuff, C., Alvarez, M., Bacon, S., Kermabon, C., 2007. Transport across the 2002 Greenland-Portual Ovide Section and comparison with 1997. Journal of Geophysical Research 112, C07003.

Lucotte, M., Hillaire-Marcel, C., 1994. Identification et distribution des grandes masses d'eau dans les mers du Labrador et d'Irminger. Canadian Journal of Earth Sciences 31, 5–13.

Mann, C.R., Coote, A.R., Garner, D.M., 1973. The meridional distribution of silicate in the western Atlantic Ocean. Deep Sea Research 20, 791–801.

McCartney, M., 1992. Recirculating components of the deep boundary current of the northern North Atlantic. Progress in Oceanography 29, 283–382.

McCave, I.N., 1983. Particle size spectra, behavior and origin of nepheloid layers of the Nova Scotian Continental Rise. Journal of Geophysical Research 88, 7647–7666.

McCave, I.N., 2001. Nepheloid layers. In: Steele, J.H., Thorpe, S.S., Turekian, K.K. (Eds.), Encyclopedia of Ocean Sciences, vol. 4. Academic Press, San Diego, pp. 1861–1870.

McCave, I.N., 2003. Nepheloid layer, sediment. In: Middleton, G.V. (Ed.), Encyclopedia of Sediments and Sedimentary Rocks. Kluwer, Dordrecht.

McCave, I.N., Tucholke, B.E., 1986. Deep current-controlled sedimentation in the western North Atlantic. In: Vogt, P.R., Tucholke, B.E. (Eds.), The Geology of North America, vol. M. Western Atlantic Region, Geological Society of America. Boulder, Co., pp. 451–468.

Millwood, L.D., Hawkins Jr. D.L., Wells, S.M., 2002. Data report: utilizing colour reflectance analysis as a carbonate concentration proxy. In: Richter, C. (Ed.), Proceedings of the Ocean Drilling Program, Scientific Results, Ocean Drilling Program, College Station, TX, p. 181.

Pickart, R.S., Straneo, F., Moore, G.W.K., 2003. Is Labrador Sea Water formed in the Irminger basin? Deep Sea Research I 50, 23–52.

Rabinowitz, P.D., Eittreim, S.L., 1974. Bottom current measurement in the Labrador Sea. Journal of Geophysical Research 79 (27), 4085–4090.

Rahmstorf, S., 2000. The thermohaline circulation: a system with dangerous thresholds? Climate Change 46, 247–256.

Rahmstorf, S., 2002. Ocean circulation and climate during the past 120,000 years. Nature 419, 207–214.

Rudels, B., Fahrbach, E., Meincke, J., Budeus, G., Eriksson, P., 2002. The East Greenland Current and its contribution to the Denmark strait overflow. ICES Journal of Marine Science 59, 1133–1154.

Saunders, P.M., 1994. The flux of overflow water through the Charlie Gibbs Fracture Zone. Journal of Geophysical Research 99 (C6), 12343–12355.

Schmitz, W.J., 1996. On the World Ocean Circulation, vol. 1. Some Global Features/North Atlantic circulation.

Schmitz, W.J., McCartney, M.S., 1993. On the North Atlantic circulation. Reviews of Geophysics 31 (1), 29–49.

Seager, R., Battisti, D.S., Yin, J., Gordon, N., Naik, N., Clement, A.C., Cane, M.A., 2002. Is the Gulf Stream responsible for Europe's mild winters? Quarterly Journal of the Royal Meterological Society 128 (B(586)), 2563–2586.

Smith, J.N., Jones, E.P., Moran, S.B., Smethie Jr., W.M., Kieser, W.E., 2005. Iodine 129/CFC 11 transit times for Denmark Strait Overflow Water in the Labrador and Irminger Seas. Journal of Geophysical Research 110 (C05006).

Spinrad, R., Zaneveld, J.R.V., 1982. An analysis of the optical features of the near-bottom and bottom nepheloid layers in the area of the Scotian Rise. Journal of Geophysical Research 87 (9533–9561).

Srivastava, S.P., Louden, K.E., Chough, S.K., Mosher, D., Loncarevic, B.D., Mudie, P.J., de Vernal, A., MacLean, B., 1989. Results of detailed geological and geophysical measurement at ODP Sites 645 in Baffin Bay and 646 and 647 in the

Labrador Sea. In: Srivastava, S.P., Arthur, M., Clement, B., et al. (Eds.), Proceedings of the Ocean Drilling Program, Scientific Results. College Station, TX, Ocean Drilling Program, vol. 105, pp. 891–919.

Stanford, J., Rohling, E.J., Hunter, S.E., Roberts, A.P., Rasmussen, S.O., Bard, E., McManus, J., Fairbanks, R.G., 2006. Timing of meltwater pulse 1a and climate responses to meltwater injections. Paleoceanography 21 (4), PA4103.

Stoner, J.S., Channell, J.E.T., Hillaire-Marcel, C., 1995. Magnetic properties of deep-sea sediments off southwest Greenland: evidence for major differences between the last two deglaciations. Geology 23 (3), 241–244.

Stow, D.A.V., Armishaw, J.E., Holmes, R., 2002. Holocene contourite sand sheet on the Barra Fan slope, NW Hebridean margin. In: Stow, D.A.V., Pudsey, C.J., Howe, J.A., et al. (Eds.), Deep-Water Contourite Systems: Modern Drifts and Ancient Series, Seismic and Sedimentary Characteristics, London. Memoir, vol. 22, Geological Society, pp. 99–119.

Swift, J.H., 1984. The circulation of the Denmark Strait and Iceland-Scotland Overflow Waters in the North Atlantic. Deep Sea Research 31, 1339–1355.

Szuman, M., Berndt, C., Jacobs, C., Best, A., 2006. Seabed characterization through a range of high-resolution acoustic systems—a case study offshore Oman. Marine Geophysical Researches 27, 167–180.

Tanhua, A., Olsson, K.A., Jeansson, E., 2005. Formation of DSOW and its hydro-chemical composition. Journal of Marine Science 57 (3, 4), 264–288.

Weiss, R., 1970. The solubility of nitrogen, oxygen and argon in water and seawater. Deep Sea Research 17, 721–735.

Wold, C.N., 1994. Cenozoic sediment accumulation on drifts in the northern North Atlantic. Paleoceanography 9 (6), 917–941.

Worthington, L.V., Volkman, G.H., 1965. The volume transport of the Norwegian Sea overflow water in the North Atlantic. Deep Sea Research 12, 667–676.